

Intra-event evolution of elemental and ionic concentrations in wet deposition in an urban environment

Thomas Audoux¹, Benoit Laurent¹, Karine Desboeufs¹, Gael Noyalet¹, Franck Maisonneuve², Olivier Laurent^{2,3}, Servanne Chevaillier²

¹ Université Paris Cité and Univ Paris Est Creteil, CNRS, LISA, F-75013, Paris, France

² Univ Paris Est Creteil and Université Paris Cité, CNRS, LISA, F-94010, Créteil, France

³ Univ Paris Est Creteil, CNRS, ENPC, Université Paris Cité, OSU-EFLUVE, F-94010, Créteil, France

Correspondence to: Thomas Audoux (thomas.audoux@lisa.ipsl.fr) ; Benoit Laurent (benoit.laurent@lisa.ipsl.fr)

Abstract.

A measurement campaign was conducted in the Paris region, focusing on the evolution of chemical composition of wet deposition during rainfall events from sequential sampling. A total of eight rain events were documented and characterized by varying meteorological conditions, atmospheric dynamics, and aerosol particle concentrations representative of urban conditions and influenced by long-range mineral dust transport. The intra-event evolution of the chemical composition of wet deposition revealed the predominant role of meteorological parameters and local sources in the observed mass concentration variability. From selected case studies, the washout ratios (WR) and scavenging coefficients were quantified by conducting simultaneous measurements of aerosol particle composition and wet deposition. The results highlighted a variability of the WR and scavenging coefficients depending on the rainfall rate and on the chemical specie. Scavenging coefficients estimated from WR ranged from 5.4×10^{-8} to $1.1 \times 10^{-5} \text{ s}^{-1}$ for chemical elements, and are within the range of values reported in the literature for 0.2-2 μm particles diameter. Our results pointed out that scavenging coefficient increases with rainfall rate according to a power law, as previously shown in the literature, indicating a stronger removal of particles from the atmosphere with greater precipitation intensity. Quantitative analysis of the data allowed us to estimate the relative contributions of in-cloud scavenging (ICS) for selected rain events. The ICS relative contributions ranged on average from 23% to 62% depending on the rain events, and varied according to the chemical species within the same rain event. This highlights the variability and complexity of the wet deposition process and the influence of specific factors on the contribution of ICS, such as aerosol particle size and hygroscopicity. Overall, this study highlights the variability of wet deposition and its chemical composition, and the need to consider the specificities of each event to fully understand the underlying mechanisms.

1 Introduction

Wet deposition involves two distinct mechanisms: in-cloud scavenging (hereafter referred to as ICS) and below cloud scavenging (hereafter referred to as BCS). ICS refers to the scavenging of aerosols within the cloud, where they either act as condensation (or ice) nuclei or are captured by already formed droplets (Seinfeld and Pandis, 2016). BCS is the result of particles being captured through collision by raindrops as they fall (Slinn, 1977). Through these two mechanisms, wet deposition includes locally emitted aerosols that can be scavenged from the

36 atmosphere, as well as long-range transported aerosols that can be removed by precipitating cloud systems (e.g.
37 Bertrand et al., 2008).

38 The proportion of ICS and BCS in wet deposition is influenced by a number of factors, including the local
39 environment (e.g. rural or urban) and associated emissions, meteorological variables such as rainfall amount,
40 intensity and type, and aerosols content in the atmosphere such as its loading, their size and vertical distributions
41 (Aikawa et al., 2014; Ge et al., 2016; Lim et al., 1991; Bertrand et al., 2008; Ge et al., 2021a). The accuracy of the
42 representation of these mechanisms in global and regional modeling is still questionable (Croft et al., 2010), as
43 there is insufficient data to constrain them accurately (Ryu and Min, 2022). Indeed, BCS was considered to be less
44 important than ICS regarding wet deposition in several modeling studies (Croft et al., 2010; Yang et al., 2015;
45 Kim et al., 2021). However, recent observation studies have found that BCS could represent a significant fraction
46 of the wet deposition (Xu et al., 2019; Ge et al., 2021a; Chatterjee et al., 2010; Karşı et al., 2018; Audoux et al.,
47 2023). Grythe et al. (2017) also emphasized the significance of BCS, indicating that it is more responsible for the
48 removal of aerosols in the lower atmosphere, while ICS dominates the wet removal in the free troposphere. These
49 recent findings demonstrate the need to re-evaluate the importance of BCS in regional and global-scale modeling
50 of atmospheric aerosols and thus the necessity to provide more in situ deposition measurements to better constrain
51 them.

52 Approaches based on only some of the measurable parameters have been used to document the scavenging of
53 atmospheric particles by precipitation. One approach is to compute the washout ratio (also called scavenging ratio
54 and hereafter referred to as WR), which is based on the ratio of the mass or elemental concentrations of wet
55 deposition to those of aerosols measured in the atmosphere (Chamberlain, 1960). WR is a parameter that integrates,
56 without distinction of processes, the relative scavenging efficiency of particulate compounds and chemical
57 elements by considering their transfer from air to water. WR has been regularly used to characterize wet deposition
58 by precipitation for different types of particulate aerosols and chemical compounds found in various atmospheric
59 environments (Jaffrezo et al., 1990; Cerqueira et al., 2010; Marticorena et al., 2017). It can also be used to estimate
60 wet deposition fluxes given air concentrations and precipitation rates (Duce et al., 1991; Mamun et al., 2022).
61 Moreover, WR make it possible to study the relative importance of some of the parameters involved in the
62 mechanism of the transfer between the phases, such as rainfall rates (González and Aristizábal, 2012) or aerosol
63 particle size (Jaffrezo and Colin, 1988; Cheng et al., 2021). However, Cheng et al. (2021) have highlighted in their
64 literature review the scarcity of particulate element WR data due to the limited co-located measurements of
65 elements in precipitation and aerosol particles. Another approach is to calculate the scavenging coefficient, which
66 is commonly used in global chemical transport models to represent the below cloud scavenging of particles by rain
67 (Ge et al., 2021b; Colette et al., 2017). Theoretical studies have primarily focused on determining the particle
68 collection efficiency of raindrops as they fall, while certain numerical, laboratory, and field studies have developed
69 semi-empirical parameterizations (Wang et al., 2014; Dépée et al., 2020; Laakso et al., 2003; Slinn, 1977).
70 However, a gap remains between field measurements, theoretical and semi-empirical parameterizations (Wang et
71 al., 2010, 2011). Therefore, the determination of both WR and scavenging coefficient appears to be very useful
72 for future wet deposition studies.

73 Several studies using sequential sampling have shown a decrease in concentration during the rain event, which is
74 more pronounced in the first few millimeters of rainfall (e.g., Seymour and Stout, 1983; Jaffrezo et al., 1990;
75 Aikawa and Hiraki, 2009). For example, Tanner et al., (2006) found that concentrations measured after 10 mm of
76 rainfall can be 2 to 33 times lower than concentrations measured in the first 2 mm of rainfall, depending on the
77 studied compounds. Sequential rainfall sampling allows the collection of successive rainfall fractions to monitor
78 the temporal variability of wet deposition (e.g., Laquer, 1990). It is of particular interest to study the dependence
79 of wet deposition content on rainfall characteristics (intensity, droplet size and distribution), which also evolve
80 during the event (Audoux et al., 2023). In addition, the study of the chemical composition of wet deposition and
81 its evolution throughout a rain event allows determining the influences of several aerosol sources (e.g.,
82 anthropogenic or natural). The intra-event evolution of rain chemical composition has also been used to discuss
83 the relative contribution of ICS and BCS mechanisms to wet deposition (e.g., Aikawa and Hiraki, 2009; Ge et al.,
84 2021; Audoux et al., 2023). Indeed, it is generally assumed that the first increments of the rain event are influenced
85 by both mechanisms, while the last fractions could be attributed to ICS only (Aikawa and Hiraki, 2009; Chatterjee
86 et al., 2010; Germer et al., 2007; Karşı et al., 2018; Desboeufs et al., 2010), although the relative proportion of ICS
87 and BCS evolves during the event (e.g., Zou et al., 2022). Therefore, studying the evolution of wet deposition
88 composition within a rainfall event provides valuable information on the temporal variability and the origin of
89 scavenged aerosol particles, both in terms of sources of pollutant and BCS and ICS mechanisms.

90 A dedicated sequential precipitation sampler as well as conditioning and chemical analysis protocols were
91 developed to document the intra-event variability of the dissolved and particulate chemical composition of rainfall
92 (Audoux et al., 2023). The present study is based on the analysis of sequential rainfall sampling performed in late
93 winter and spring 2022 at a study site in the Paris region, which included eight case studies with contrasting
94 meteorological conditions, atmospheric loading, and chemical composition. It has two objectives: (1) to document
95 the intra-event evolution of ionic and elemental composition of dissolved and particulate phase species in wet
96 deposition for contrasted rain events and (2) to discuss the parameters influencing wet deposition chemistry
97 through the quantification of washout ratios and scavenging coefficients and the estimation of the relative
98 contribution of BCS and ICS mechanisms in the wet deposition.

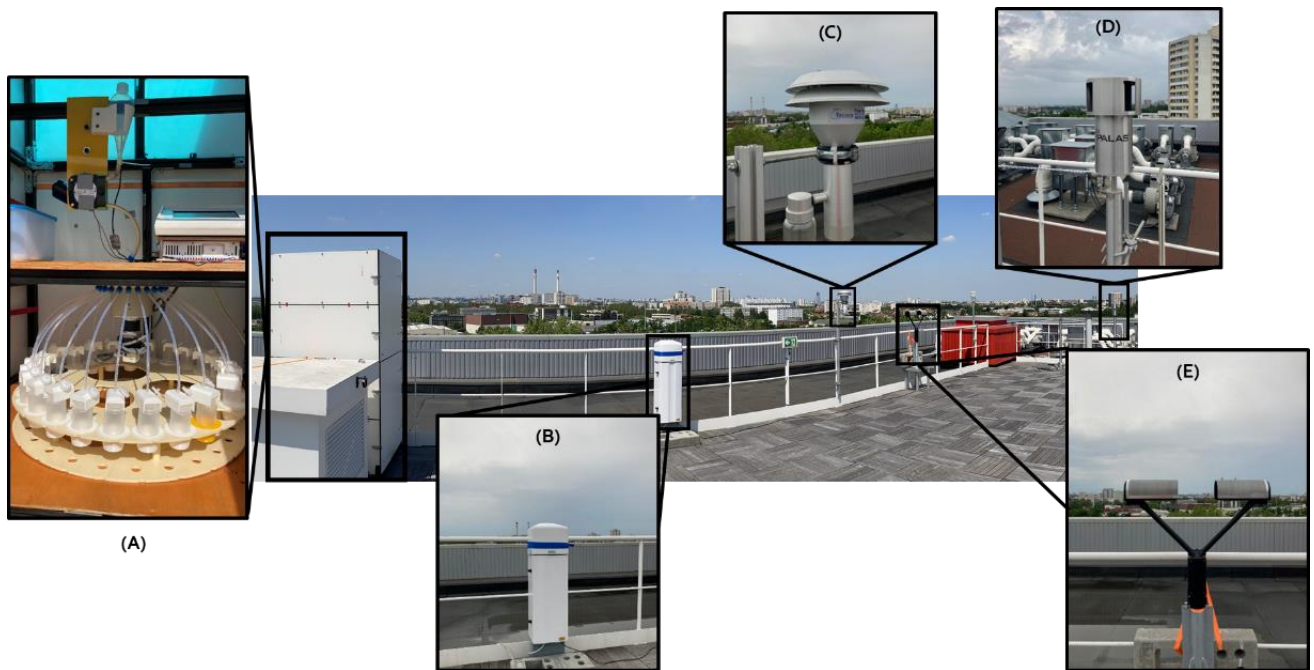
99 **2 Material and methods**

100 **2.1 Measurement site and sampling strategy of wet deposition and aerosol particles**

101 The sampling site is located at the air quality station operated by the Interuniversity Laboratory of Atmospheric
102 Systems (LISA), which is inside the University of Paris Est Creteil (UPEC) in the south-east of the Paris
103 agglomeration (48.79 °N-2.44 °E) (Figure 1). The study site is in close proximity to various sources of pollution
104 including nearby industries and an incinerator, highways, railway stations, and construction sites. Between July
105 2021 and July 2022, daily rainfall depths measured using a Précis-Mécanique rain gauge model 3 070 A (0.2 mm
106 precision) at the study site ranged from 0.2 to 37.6 mm. 19% of rainy days presented rainfall depths lower than
107 0.4 mm, 12% were between 0.4 and 1 mm, 40% were between 1 and 5 mm, and 13% were higher than 10 mm.
108 The sampling strategy is to investigate case studies sampled during an intensive measurement campaign during
109 the winter and spring of 2022. During this period, the daily average PM₁₀ (PM_{2.5}) concentrations were around 17.5

110 (11.2) $\mu\text{g m}^{-3}$ with values reaching up to 57.5 (43.0) $\mu\text{g m}^{-3}$. Wet deposition collection is performed with a
111 sequential sampler specifically developed at the LISA (Figure 1 A). Sampling, conditioning and analysis of rain
112 samples are described in detail in Audoux et al. (2023), and thus, it is briefly reminded here.

113 The rain is collected using a Teflon pyramid funnel with a collection surface of 1 m² in combination with a
114 sampling unit. This unit enables the automatic collection of up to 24 consecutive fractions of rain, adjustable from
115 0.05 to 2.0 mm, to study dissolved and particulate phase of the wet deposition. The sampling is conducted based
116 on volume, and as a result, it is dependent on the rainfall rate. The sequential sampler is able to correctly collect
117 rainfall fractions for low rainfall intensities, as well as for more intense rainfall recorded by the rain gauge and
118 disdrometer, in comparison with standardized measurements (Audoux et al., 2023). The materials that make up
119 the sampler have been chosen to allow analysis of the ionic and elemental composition of the dissolved and
120 particulate phase at high and low concentration levels (from several mg L⁻¹ to hundreds of ng L⁻¹). The sampling
121 bottles and materials that came in contact with the samples underwent a thorough washing protocol in clean-room
122 laboratory with ISO 7 and ISO 5 level controls.



123

124 **Figure 1: Study site. (A) Rain sequential sampler; (B) Ceilometer; (C) PM₁₀ inlet for filter sampling; (D) FIDAS; (E)**
125 **Disdrometer**

126 A summer rain event was collected in July 2021 (R1) and a winter rain event were collected in February 2022 (R2)
127 (Audoux et al., 2023). These case studies are completed here with 6 additional events collected in late winter and
128 spring 2022, between March (R3, R4, R5, R6 and R7 rain events) and April (R8 rain event). For the 8 rain events
129 studied, between 11 and 32 consecutive fractions have been sampled, the latter being collected within 10 seconds
130 to 2 hours, depending on the rainfall rate.

131 Concomitant measurements on atmospheric aerosols and meteorological parameters during the rain sampling is
132 important for a more in-depth understanding of wet deposition mechanisms. Therefore, PM_{2,5} and PM₁₀ aerosol

133 mass concentration, as well as the particle size distribution (PSD) between 0.18 and 18 μm , are measured using
134 the FIDAS (Figure 1 D), equipped with a TSP Sigma 2 inlet, with a 1 min time step. The FIDAS is an instrument
135 used for regulatory air quality measurement of $\text{PM}_{2.5}$ and PM_{10} mass concentration (LCSQA, 2021). Moreover,
136 PM_{10} aerosol particles are sampled on polycarbonate membranes (Nuclepore®, 0.4 μm porosity) using a PM_{10}
137 head sampling (Figure 1 C). Air sampling is done between 15 hours and 24 hours before the start of the rain and
138 is stopped at the beginning of the latter, within one minute after removing the cover from the sequential sampler,
139 while the first fraction is being collected. This allows characterizing the chemical composition of the atmospheric
140 aerosol prior to rainfall. Rainfall rate and droplet size distribution (DSD) are measured using an OTT PARSIVEL®
141 (PARticle Size and VELOCITY, Figure 1 E, Supplement 1) optical disdrometer with a time resolution of 30 seconds.
142 In parallel, wind direction, wind speed as well as air temperature and relative humidity are measured using
143 instrumentation from Campbell Scientific© and are recorded with a time step of 1 min. The cloud base height and
144 homogeneity of atmospheric column are measured using a ceilometer (Vaisala CL31, Figure 1 B, Supplement 2).
145 Parsivel disdrometers and ceilometers are typically used in multiple measurement networks for precipitation and
146 cloud base height characterization (e.g., Haeffelin et al., 2005; Tapiador et al., 2010). FIDAS, ceilometer and
147 disdrometer measurements are made continuously at the study site, while aerosols filter sampling and deposition
148 measurements are made on alert before or during rain events. This makes it necessary to regular follow-up the
149 precipitation alerts.

150 **2.2 Elemental and ionic composition analysis of wet deposition and atmospheric aerosol**

151 After sampling, rain samples are quickly processed for ionic and elemental analysis, usually within a time frame
152 of 1 to 12 hours after the end of rainfall. If immediate processing is not feasible, the samples are kept in a cool and
153 dark environment at 6° C, and are processed within 24 to 48 hours. Treatment, filtration, and conditioning are done
154 in a clean-room laboratory with ISO 6 level controls, under a laminar flow hood (U15 filter) which is estimated to
155 be equivalent to ISO 3. A pH meter (METTLER TOLEDO Seven2Go) is used to measure the pH of each sequential
156 sample. Samples are then filtered through pre-cleaned Nuclepore® polycarbonate membranes with a porosity of
157 0.2 μm to separate the particulate phase from the dissolved phase. Following Audoux et al. (2023), the dissolved
158 phase is then divided into two fractions. The first fraction (10 mL aliquot) is frozen until the analysis of water-
159 soluble major inorganic cations (Na^+ , NH_4^+ , K^+ , Mg^{2+} , Ca^{2+}), anions (Cl^- , NO_3^- , PO_4^{3-} , SO_4^{2-}) and organic ions
160 (HCOO^- , CH_3COO^- , $\text{C}_2\text{H}_5\text{COO}^-$, MSA, $\text{C}_2\text{O}_4^{2-}$) by Ion Chromatography (Compact IC Flex, Metrohm®,
161 PRAMMICS Platform). The second fraction (two 15 mL aliquots) is acidified to pH = 1 with nitric acid
162 (Suprapur®) and stored at 6° C until analysis of water-soluble Al, Ba, Ca, Cr, Fe, K, Mg, Mn, Na, Ni, P, S, Si, Ti
163 and Zn by Inductively Coupled Plasma Atomic Emission Spectrometer (ICP-AES, Spectro ARCOS Ametek®).
164 The membranes are dried under laminar flow hood and conditioned for 48 h at a constant relative humidity of 45
165 – 50% and at $T = 20^\circ\text{C}$ prior weighting using a precision microbalance (METTLER TOLEDO® XPR26C,
166 PRAMMICS Platform). In order to accumulate a sufficient amount of material for analysis, several rain sequential
167 samples can be filtered through the same filter. Conversely, when the particulate load is too high, rain fractions
168 can be filtered through multiple membranes. Elemental composition (Al, Ba, Ca, Cr, Fe, K, Mg, Mn, Na, Ni, P, S,
169 Si, Ti, and Zn) of the particulate phase is determined using X-ray fluorescence spectrometer (XRF, ZETIUM 4
170 kW, Malvern Panalytical, PRAMMICS Platform). The 0.4 μm porosity Nuclepore® membranes are also analyzed
171 using XRF to characterize the elemental composition of the aerosol in the air prior to rainfall events. Our strategy

172 is to monitor the elemental inorganic fraction of the aerosol in order to link it to the rainfall composition. It
173 therefore allows us to characterize about 40% of the average aerosol composition in the Paris region (Airparif,
174 2021).

175 **2.3 Origin of scavenged aerosol particles**

176 The origin of scavenged aerosol particles can be discussed in relation with their chemical compositions and the
177 trajectory of the air masses. We calculated enrichment factors (EFs, Taylor and McLennan, 1985) in order to
178 determine the origin of elements found in the rain samples. Al is used as the reference of the Earth's crust (hereafter
179 referred to as EF_X^{crust}), and Na as reference of the sea salt (hereafter referred to as $EF_X^{sea\ salt}$). Equation 1 is used
180 to calculate EF as follows:

$$181 \quad EF_X(\%) = \frac{([X]/[ref])_{rain}}{([X]/[ref])_{crust\ or\ sea\ salt}} \times 100 \quad (1)$$

182 Where $([X]/[ref])_{rain}$ correspond to the ratio between the element X and the reference (Al or Na) concentrations
183 in rainwater samples and $([X]/[ref])_{crust\ or\ sea\ salt}$ the concentrations in the continental crust or in the sea.

184 To complement local wind measurements at the study site, air mass trajectories were calculated using the
185 HYSPLIT model (<https://ready.arl.noaa.gov/HYSPLIT.php>) (Draxler and Rolph, 2012). HYSPLIT is a retro-
186 trajectory analysis used to study local to continental air mass dispersion and transport of atmospheric compounds,
187 respectively (Celle-Jeanton et al., 2009; Bertrand et al., 2008; Calvo et al., 2012), and to determine the origin of
188 air masses to identify sources of atmospheric substances, e.g., mineral dust, sea salt or anthropogenic (Vincent et
189 al., 2016; Anil et al., 2017). Here, 48 h or 120 h depending on the event, backward trajectories were computed by
190 the HYSPLIT model with GFS (0.25 °, global) from the study site (47.79 °N - 2.44 °W) at the surface (0 m a.g.l.)
191 and at the cloud base height measured by the ceilometer.

192 **2.4 Determination of washout ratios, scavenging coefficient and scavenging mechanism contributions**

193 2.4.1 Washout ratios

194 The washout ratio is a parameter used to quantify the relative scavenging efficiency of particulate chemical
195 elements by rain. It is based on the principle of a transfer of the compounds from the air to the water. Therefore,
196 below cloud WR are determined from the ratio of the elemental concentration measured in the wet deposition
197 (C_{rain}) to those measured in the air (C_{air}) (equation 2).

$$198 \quad WR = \frac{C_{rain}(\mu g\ kg^{-1})}{C_{air}(\mu g\ m^{-3})} \times \rho_{air}(kg\ m^{-3}) \quad (2)$$

199 Here, instead to use the whole event for calculation of the WR (equation 2) as in the literature (e.g., Cheng et al.,
200 2021), the sequential sampling enables to use the concentration measured in the first fraction of the rainfall, that
201 is, the one mainly controlled by the BCS. That is more relevant regarding aerosol scavenging and determination
202 of below-cloud WR, since this allows to avoid being affected by the dilution effect reported in the literature (e.g.,
203 Jaffrezo et al., 1990).

204 In order to discuss the relationship between aerosol and wet deposition, information is needed on both aerosol and
205 rain, which we have for R2, R3, R5 and R8. To accurately calculate the WR, it is important to consider the
206 homogeneity of the atmospheric column to ensure the representativeness of surface aerosol measurements. In our
207 study, we observed the presence of a high-altitude aerosol layer using ceilometer measurements (Supplement S2).
208 The atmospheric transport of mineral dust at high altitudes rendered the collected aerosol sample unrepresentative
209 of the scavenged air column. As a result, we excluded the R5 study case from the WR calculation. Therefore, we
210 will focus our discussion on the WR of the element only for R2, R3, and R8.

211 2.4.2 Scavenging coefficient

212 We can determine the scavenging coefficient (Λ , s^{-1}) of elements using field measurements and based on the
213 estimation of their washout ratios, as previously done in the literature for sulfate, nitrate and ammonium (Okita et
214 al., 1996; Xu et al., 2019; Andronache, 2004; Yamagata et al., 2009). Indeed, by assuming a uniformly mixed
215 atmospheric column below the cloud base, the average scavenging coefficient of elements can be expressed using
216 equation (3), R and H being the rainfall rate (in $mm\ s^{-1}$) and the average cloud base height (in m) during the first
217 fraction of rainfall, respectively.

$$218 \quad \Lambda (s^{-1}) = WR \times \frac{R}{H} \quad (3)$$

219 2.4.3 In-cloud vs. below-cloud scavenging

220 The relative contribution of the ICS mechanism to the measured wet deposition is determined by analyzing the
221 mass concentrations of chemical species measured at the end of rainfall (referred to as C_{ICS}). Indeed, due to the
222 scavenging during the initial stages of rainfall, the end of rainfall is characterized by lower PM concentration,
223 which makes the BCS mechanism negligible in terms of wet deposition (e.g., Aikawa and Hiraki, 2009) since the
224 rain composition can be considered representative of the concentrations of droplets in the cloud. Different
225 approaches are used to determine C_{ICS} , such as measuring after a certain amount of rainfall (e.g., 5 mm; Aikawa
226 and Hiraki, 2009; Xu et al., 2017) or selecting the lowest values during rainfall events (Karşı et al., 2018; Berberler
227 et al., 2022). Some authors also fit an exponential decay law and use the constant value as C_{ICS} (Ge et al., 2021a),
228 while others determine C_{ICS} using the average value obtained during periods of lower mass concentration variations
229 (Chatterjee et al., 2010). In our case, we selected rainfall events for which the measurements indicated an effective
230 scavenging of the atmospheric column, with a predominant relative contribution of ICS at the end of the event. To
231 select these events, we used the following criteria: 1) the decrease of concentrations measured in the wet
232 deposition, reflecting the evolution of the contribution of the BCS; 2) the decrease of atmospheric concentrations
233 measured using the FIDAS, suggesting a progressive scavenging of the air column under the cloud; and 3) constant
234 concentrations of wet deposition at the end of the event, indicating a steady state between ICS and BCS. From
235 these criteria, the relative contributions of the scavenging mechanisms could be discussed for R1, R2, R4 and R8
236 case studies.

237 We determine C_{ICS} , using the VWM of the last fraction of rain, once a steady state is reached at the end of the
238 rainfall for R1 (1.48–2.65 mm), R2 (1.02–1.33 mm for SNA and 0.89–1.33 mm for other elements), R4 (2.21 –

239 4.42 mm) and R8 (1.87 – 6.94 mm). The wet deposition flux due to the ICS mechanism can thus be calculated
240 using C_{ICS} and P_{tot} , the total rainfall depth of the rainfall (equation 4) as done previously in the literature (Xu et
241 al., 2017; Aikawa et al., 2014; Ge et al., 2021a).

$$242 F_{ICS} = C_{ICS} \times P_{tot} \quad (4)$$

243 Then, the wet deposition flux due to BCS mechanism (F_{BCS}) is determined by subtracting F_{ICS} from the total
244 (dissolved + particulate) wet deposition (F_{total}). Relative contributions of BCS (BCS_C) and ICS (ICS_C) to wet
245 deposition can be obtained using equations 5 and 6, respectively.

$$246 BCS_C = \frac{F_{BCS}}{F_{total}} \quad (5)$$

$$247 ICS_C = \frac{F_{ICS}}{F_{total}} \quad (6)$$

248 3. Results

249 3.1 Description of wet deposition case studies

250 Eight rainfalls constitute a data set illustrating various cases in terms of aerosol concentrations and compositions
251 as well as precipitation properties. The properties of the 8 rainfall events studied are listed in Table 1. The rainfall
252 events are characterized by variable rainfall depths ranging from 0.9 to 6.9 mm and mean rainfall rate from
253 0.4 mm h⁻¹ to 11.5 mm h⁻¹. Depending on the rainfall depths and rates, the sampling resolution was adapted. For
254 example, R7 was collected in 22 fractions of volumes ranging from 80 to 440 mL for a rainfall depth of 3.04 mm
255 over 30 min, while R8 was collected in 32 fractions of volumes ranging from 60 to 820 mL for a rainfall depth of
256 6.9 mm and lasted several hours. Note that for R7, the sampling setup allowed us to only collect the first 3.04 mm
257 of rain of the total event (10.3 mm). Our dataset consists of one (12.5%) event with a rainfall depth of less than
258 1 mm, one (12.5%) with a rainfall depth of more than 5 mm and the other (75%) representing rainfall depths
259 between 1 and 5 mm. Rain events have varying cloud base heights (from 200 m for R6 up to 2 000 m for R8)
260 which, however, can fluctuate within the same event as it is the case for R8.

261 According to the HYSPLIT 48 h back trajectory calculation, the origin of the air masses scavenged at the study
262 site remained constant during the duration of the rain events, except for R6 and R8 (Supplement S3). The air
263 masses for R1 and R2 came from the Atlantic Ocean. R3 and R4 had air masses from the Mediterranean at the
264 surface and from Spain and Portugal at the cloud base. For the other events, influenced by mineral dust intrusion
265 from North Africa, the calculation of HYSPLIT back trajectories has been performed over 120 hours with the
266 same conditions. For R5 and R6, the air masses at the surface came from the United Kingdom via the North Sea
267 and Germany, while the air masses at the cloud base came from North Africa (south of Tunisia/west of Libya) for
268 R5 and from the Mediterranean Basin and Italy for R6. In the second phase of the event R6 (after 9:00 UTC), the
269 air masses at the surface also came from the Mediterranean Basin. For R7, the air masses at the cloud base came
270 from the Mediterranean Basin and the air masses at the surface came from Libya. For R8, the beginning of the
271 event was characterized by air masses coming from the Atlantic through North Morocco and Spain at the cloud

272 base and from northern Tunisia at the surface. During the event, the origin of air masses evolved and came from
 273 different places in Northern Africa (Morocco, Algeria, and Tunisia) depending on altitude. This analysis of the
 274 back trajectories shows a close alignment between the origins of these large-scale air masses and the wind
 275 directions measured at the surface at the instrumented site in Creteil.

276 Atmospheric aerosol mass concentrations at the beginning (average over the 30 min prior to the onset of the
 277 rainfall) of R1, R2, R6 and R7 events are primarily controlled by PM_{2.5}, which represents 63–84% of PM₁₀
 278 concentrations. R3 is characterized by a lower proportion of PM_{2.5}, which represents 38% of PM₁₀, while PM_{2.5}
 279 measured for R4, R5 and R8 correspond to 46–53% of PM₁₀. R1 to R4 took place on days with low particle
 280 concentrations, with PM₁₀ concentrations lower than of 20 µg m⁻³. During these events, rain had the effect of
 281 reducing atmospheric PM₁₀ concentrations by 11–53% (Table 1). However, this illustrates the overall effect of the
 282 rain event without taking into account the increases in air concentrations that may have been observed during the
 283 events (e.g., R8). On the other hand, R5 to R7 occurred on days marked by high concentrations of both PM_{2.5} (33–
 284 40 µg m⁻³) and PM₁₀ (47–63 µg m⁻³). The latter took place not only during a typical spring pollution episode (Favez
 285 et al., 2021), but also during a mineral dust intrusion from North Africa, as shown by a multi-model dust optical
 286 depth simulation provided by the WMO Barcelona Dust Regional Centre (Supplement S34, <https://dust.aemet.es>,
 287 Basart et al., 2019). During these events, rain was less effective at reducing PM₁₀ concentrations. While R5 is
 288 characterized by a decrease in the PM₁₀ concentration of the order of 17%, R6 and R7 show no variation or an
 289 increase in the PM₁₀ concentration (Table 1). Even though R8 occurred on a day with low particle concentrations,
 290 this event was also marked by the intrusion of mineral dust from northern Africa (Supplement S4, Table 1).

291 Total wet deposition fluxes in our case studies are ranging from 11 to 107 g m⁻² and are not correlated with rainfall
 292 depth nor rainfall rate (Table 1). Indeed, higher wet deposition fluxes are observed for rainfall events (R5 and R6)
 293 associated with low rainfall depth but higher pre-rain PM₁₀ concentration. However, events characterized by a
 294 similar surface PM₁₀ mass concentration (R1, R2, R3, R4 and R8) exhibit total wet deposition fluxes that vary
 295 over a factor 4.

296 **Table 1. General information of studied rainfall events.**

Period Date, Hour (UTC)	Rain	Number of rain fractions	Rainfall depth (mm)	Mean rainfall rate (mm h ⁻¹)	Pre-rain PM ₁₀ concentration (µg m ⁻³)	PM _{2.5} /PM ₁₀ fraction (%)	After-rain PM ₁₀ concentration (µg m ⁻³)	Origin of air masses	Cloud base height (m)	Total wet deposition fluxes (g m ⁻²)	pH range
Jun.27 6:55 – 12:25	R1	21	2.65	0.48	18.7	61	12.2	West	-	11.3	5.0 – 6.0
Feb.10 17:28 – 20:55	R2	17	1.33	0.49	13.0	70	6.1	West	500 – 1 000	12.0	6.3 – 6.8
Mar.11 11:06 – 13 :19	R3	15	1.03	0.69	11.8	36	9.0	South-South West	2 000	25.7	7.8 – 7.1
Mar.11 14:16 – 17:24	R4	17	4.42	1.41	9.9	55	4.6	South	1 200 – 1 500	27.8	6.0 – 6.9
Mar.29 13:10 – 16:50	R5	11	0.90	0.40	62.6	52	52.1	North-East (surface) South (cloud base)	1 500 – 2 000	106.3	7.8 – 8.4
Mar.30 4:55 – 9:31	R6	15	1.20	0.43	44.3	82	51.7	South	200	107.1	7.2 – 8.0

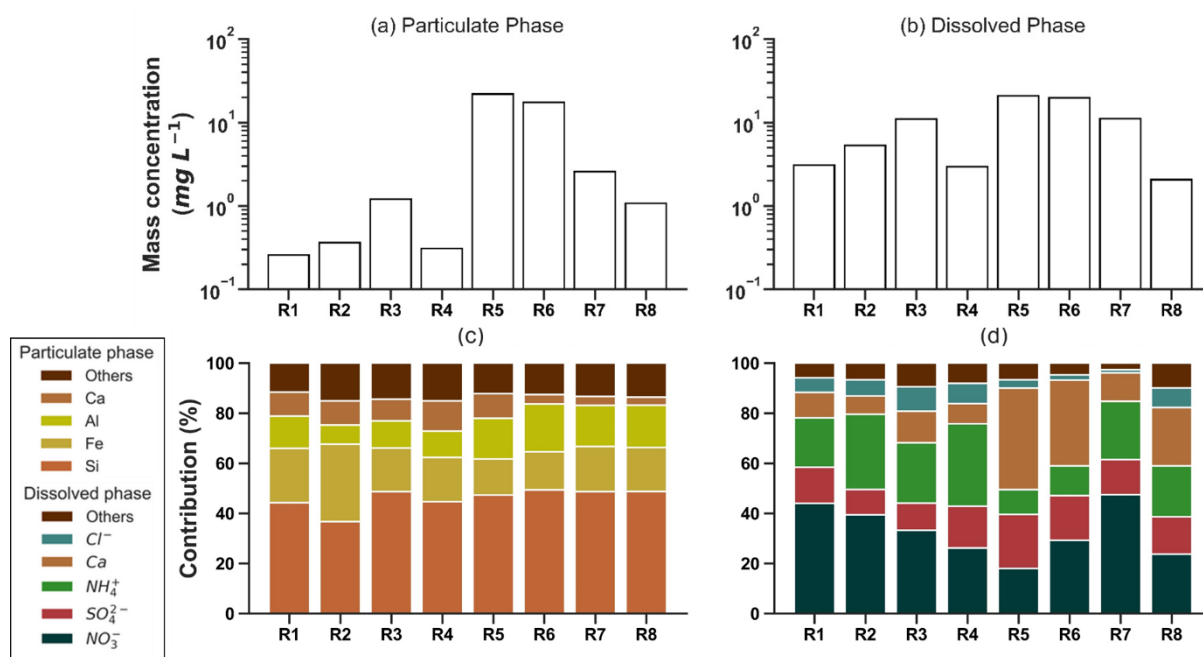
Mar.30 15:32 – 16:01	R7	22	3.04	11.5	47.2	80	46.6	South	1 000	69.0	6.6 – 7.4
Apr.13 3:00 – 12 :12	R8	32	6.94	0.90	11.9	46	10.6	South	200 – 2 000	47.9	6.1 – 7.1

297 The information collected makes it possible to describe 8 case studies, illustrating contrasting situations in terms
 298 of meteorological conditions, dynamics and atmospheric aerosol loads.

299 3.2 Classification of case studies

300 Volume weighted mean (VWM) mass concentrations of the particulate and dissolved phases for each rain event
 301 are represented in figure 2.

302 Regarding the particulate phase, the average mass concentrations of elements in the rainfall exhibit high variation,
 303 with values differing by a factor of 85 between events. The highest concentrations are observed for R5 and R6
 304 events, with 33.9 and 34.5 mg L⁻¹, respectively. Despite these fluctuations in average mass concentrations, the
 305 particulate phase is predominantly composed of Si, Fe, and Al, contributing to a relative proportion between 73%
 306 and 85%. In contrast, the particulate Ca content displays a more pronounced variability, ranging from 3% to 12%
 307 depending on the specific rain event.



308
 309 **Figure 2. Volume weighted mean mass concentrations (mg L⁻¹) of (a) particulate and (b) dissolved phases. Contribution**
 310 **of elements in the elemental composition of particulate phase (c) and of chemical species of ionic and elemental**
 311 **composition of dissolved phase (d).**

312 Regarding the dissolved phase, R4 and R8 are the rainfall events characterized by the lowest dissolved phase
 313 VWM concentrations (~ 2 to 3 mg L⁻¹) and the largest rainfall amounts (4.4 mm and 6.9 mm for R4 and R8,
 314 respectively). These results are consistent with the dependence of wet deposition concentrations with precipitation
 315 amount and the dilution effect documented in the literature (e.g., Jaffrezo et al., 1990). The largest concentrations
 316 are of the order of 21 mg L⁻¹ and correspond to the events marked by the mineral dust intrusion from northern

317 Africa but also the lowest precipitation amounts (0.90 mm for R5 and 1.20 mm for R6). The rain events are not
 318 characterized by the same contents and relative proportions of acid (NO_3^- , SO_4^{2-}) or neutralizing (NH_4^+) species
 319 depending on the rainfall. The dissolved phase is mainly composed of SO_4^{2-} , NO_3^- and NH_4^+ (SNA), between 58
 320 and 85% by mass of the analyzed species for R1, R2, R3, R4, R7 and R8. In contrast, R5 and R6, and to a lesser
 321 extent R8, are composed of a non-negligible proportion of Ca in the dissolved phase (23 – 40%).

322 The variations in concentrations of not only acid species, but also neutralizing compounds, lead to different pH
 323 values in the rainfall (Table 1). The progressive scavenging of these compounds during the rainfall event also
 324 results in variations in pH (Asman et al., 1982), which is observed between the different events. For instance, R1
 325 has a lower pH ($\text{pH} < 5.6$) resulting from lower average concentrations of neutralizing species. Rains R2, R3, R4,
 326 R7 and R8 have higher pH values ranging from 6.2 to 6.8, and even basic for R5 and R6 (7.5 – 8.0). The basic
 327 nature of R5 and R6 rains is attributed to the higher Ca contents of mineral dusts present in these rains, which is
 328 in agreement with the influence of dust intrusion, as previously described (Ma, 2006; Oduber et al., 2020).

329 To go further in the interpretation, EFs presented in table 2 as well as origin of air masses (Table 1), are used to
 330 classify case studies into three groups: (i) R1 to R4, characterized by air masses from the west and south of France
 331 and a significant enrichment in Ca ($\text{EF} > 15$), Ni ($\text{EF} > 10$, except R4), P ($\text{EF} > 30$, except R1) and very high for Zn
 332 ($\text{EF} > 120$) and S ($\text{EF} > 1\ 000$); (ii) R5 and R6, characterized by a contribution of mineral dust and EFs reflecting
 333 mineral sources signature (between 1 and 2), except for Zn (8.0 – 13) and S (119 – 136), which are still lower than
 334 the other rains; and (iii) R7 and R8, characterized by low EFs (< 10) for all elements, but higher than R5 and R6
 335 ones, except for Zn (26 – 44) and S (175 – 438).

336 **Table 2. Enrichment factors (EF^{crust}) of elements measured in the rain events relative to the upper continental crust.**
 337 **Bold values indicate significant enrichment of the element ($\text{EF}^{\text{crust}} > 10$).**

EF^{crust}	Ba	Ca	Cr	Fe	K	Mg	Mn	Na	Ni	P	S	Sr	Ti	V	Zn
R1	7.9	19	5.6	2.5	3.2	1.4	3.8	4.8	17	8.1	1 281	5.4	1.7	2.6	226
R2	20	31	16	6.3	12.7	1.0	9.3	16	52	53	1 853	9.9	4.2	16	396
R3	6.6	25	5.2	2.6	5.9	1.8	5.4	13	11	33	1 060	6.3	3.0	5.0	121
R4	7.5	17	5.6	2.7	7.0	1.5	5.2	9.9	5.4	38	1 521	5.2	3.0	14	190
R5	2.6	6.6	2.3	1.4	1.2	1.0	1.5	0.37	0.9	3.8	136	2.8	1.7	3.1	13
R6	2.1	4.4	1.8	1.3	1.1	0.92	1.2	0.25	2.2	1.4	119	2.0	1.5	2.6	8.0
R7	4.2	7.1	4.1	1.8	1.6	1.1	1.9	0.53	3.7	4.1	438	2.7	1.8	3.1	44
R8	3.2	6.2	2.9	1.7	1.7	1.1	1.8	1.6	5.1	3.2	176	2.1	1.8	3.3	26

338 The chemical signature allows us to classify rain events into three categories: R1, R2, R3 and R4 show a marked
 339 anthropogenic signature and are hereafter referred to as “anthropogenic” events; R5 and R6 illustrate a distinct
 340 mineral dust signature and hereafter referred to as “mineral-dust” events; when R7 and R8 correspond to mixing
 341 conditions and are hereafter referred as “mixed” events. However, for a given element, the EF show that the origin
 342 is sufficiently homogeneous regardless of the rain events, limiting the data analysis as a function of aerosol sources.

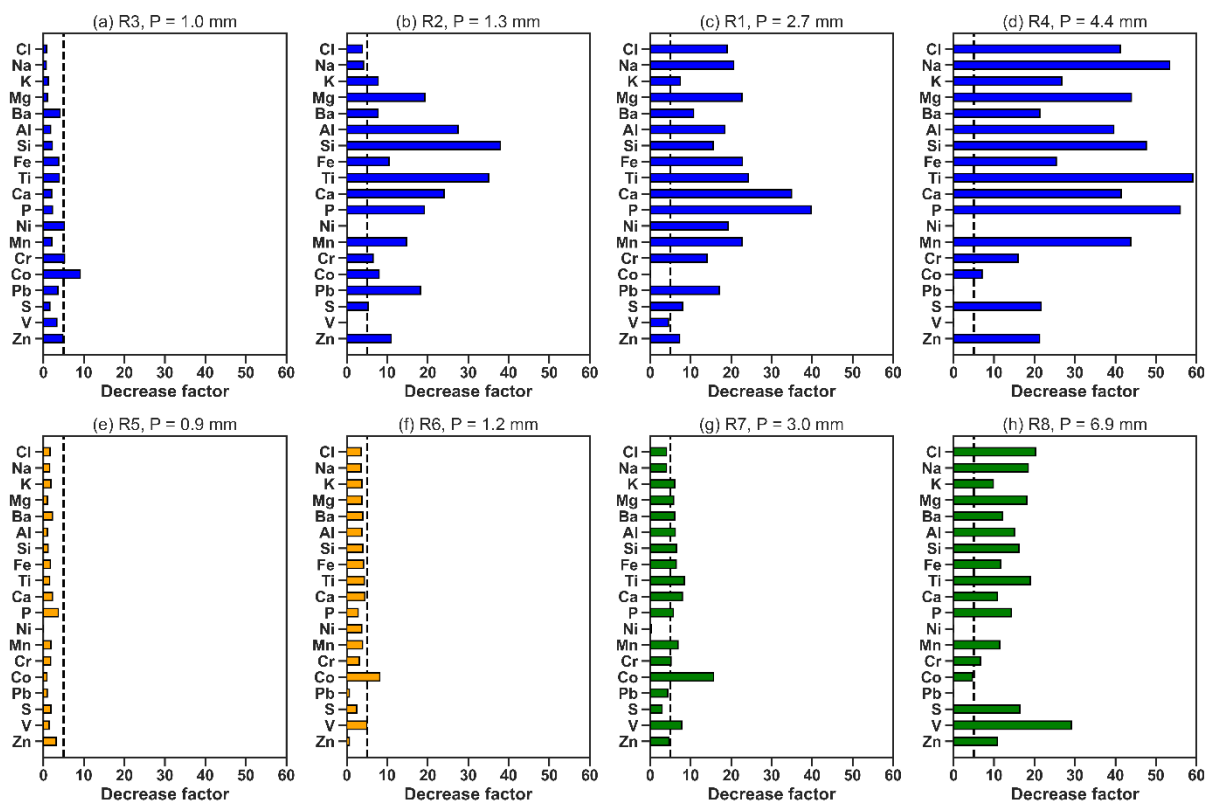
343 **4. Discussion**

344 **4.1. Sequential wet deposition composition**

345 4.1.1. Overall decrease of mass concentration

346 We firstly quantify for each event an overall decrease in mass concentrations of the particulate (up to a factor of
347 50) and dissolved (up to a factor of 35) phases, without distinction of the chemical composition (Supplement S5).
348 The decrease factors (DF) is computed for each rain as the ratio of the mass concentration of the first fraction to
349 the last fraction of rainfall. DF were 1.4 (R8) to 7.3 (R2) times higher for the particulate phase than for the dissolved
350 phase, depending on the event. This is consistent with a more efficient scavenging of coarse particles (Al, Fe and
351 Si), constituting a significant share of the particulate mass concentration (Figure 2), compared to the secondary
352 submicronic aerosols (SNA) that make up a large proportion of the dissolved phase (Figure 2), as previously
353 observed in the literature.

354 Overall, we found that for a given type of rain (“anthropogenic” Figure 3 a, b, c and d, “mineral-dust” Figure 3 e
355 and f, or “mixed” Figure 3 g and h), in other words, for atmospheric content of the same order of magnitude and
356 for similar chemical composition (see Table 1 and Figure 2), the DF increases with rainfall depth (Figure 3). In
357 addition, R5 and R6 were characterized by high atmospheric aerosol concentrations and a long-range transport of
358 mineral aerosols at altitude and low rainfall rate ($< 0.5 \text{ mm h}^{-1}$). The latter explain the low DF, due to high mass
359 concentrations observed throughout the event due to both the low decrease of atmospheric content and the
360 additional contribution of dust particles within the clouds. Within a given event, elemental DF exhibits significant
361 variability depending on the element (Figure 3), even when elements share a similar predominant phase and similar
362 size characteristics. For example, in the case of R4 event, DF of Cl is two times higher than S, while they are
363 predominantly in the dissolved phase, and DF of Ti is almost 4 times higher than Cr, while they are predominantly
364 in the particulate phase. These observations underline the importance of considering individual element behaviors
365 when assessing wet deposition dynamics.



366

367 **Figure 3. Element decrease factor (DF) for each rain event. The dotted line marks a DF = 5. Missing bar means that the**
 368 **concentration in the first fraction and/or the last fraction of rainfall is below detection limit. Blue bars, orange bars and**
 369 **green bars correspond to “anthropogenic”, “mineral-dust” and “mixed” events, respectively.**

370 4.2.2. Intra-event evolution

371 Sequential sampling enabled the observation of various patterns of concentration evolution during rainfall events.
 372 Some events were characterized by a continuous decrease in mass concentrations throughout the rainfall,
 373 ultimately reaching a lower and constant level in the final fractions regardless of the phase nor the chemical species
 374 (R1, R7). This kind of evolution is commonly found in the literature, with a high-decreasing trend in the first 1 to
 375 3 mm, until reaching a constant level until the end of the rainfall, for both dissolved and particulate phases (e.g.,
 376 Jaffrezo et al., 1990; Kasahara et al., 1996). In contrast, although lower and constant levels were reached at the
 377 end of rainfall, R4, R5 and R8 exhibited punctual increases or stabilization of the concentrations of both phases
 378 during the rainfall, while R2, R3 and R6 events showed only punctual increases of the dissolved phase.

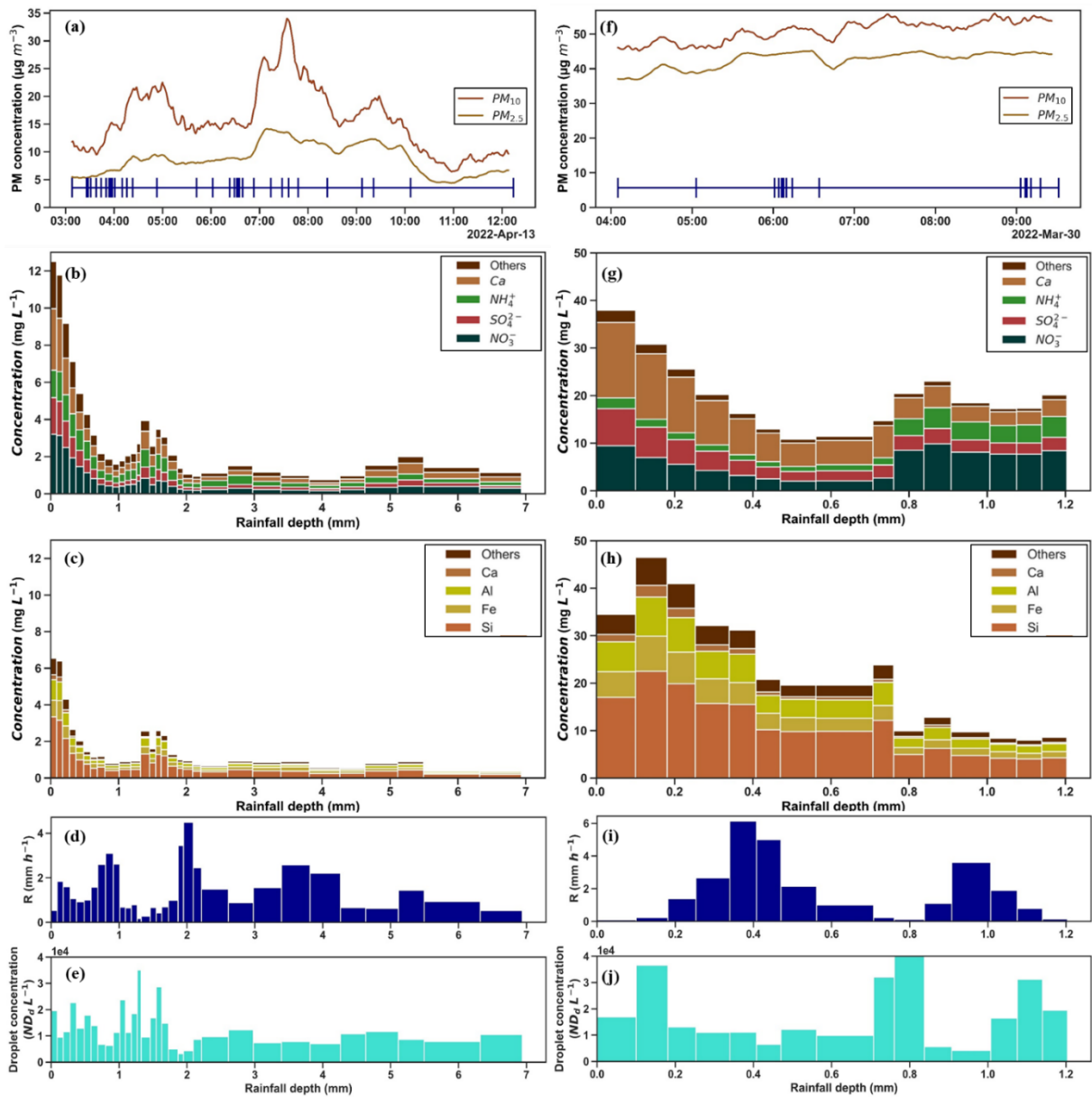
379 As an illustration, Figure 4 shows the temporal evolution of atmospheric concentrations (PM_{10} and $PM_{2.5}$), the
 380 evolution of mass concentrations of dissolved and particulate phases, rainfall intensity and droplet concentrations
 381 (i.e., the number of droplets measured by the disdrometer divided by the unit of volume of the collected rain
 382 fraction) during R6 and R8 events. It has been observed that atmospheric concentrations evolve differently
 383 according to particle size classes ($PM_{2.5}$ vs. $PM_{2.5-10}$) and rainfall phases. Generally, precipitation is associated with
 384 a decrease in atmospheric concentrations during rainfall (Table 1), except for event R6 (Figure 4f). However, an
 385 increase in concentrations of the coarse aerosol fractions ($PM_{2.5-10}$) is observed quite systematically as rainfall
 386 intensities decrease below 0.5 mm h^{-1} , especially for events R2, R4, and R8 (between 4:00 and 5:00) as shown in
 387 Figure 4a.

388 Increase of wet deposition concentrations during rainfall has been previously observed by some authors (e.g., Karşı
389 et al., 2018). Here, since the latter were systematically correlated with a decrease in precipitation intensity
390 (Figure 4d, i) and an increase in droplet concentration (Figure 4e, j). Several possible explanations are considered
391 for these observations: this could either be due to an effect of "over-concentration" of falling raindrops or a release
392 of aerosols due to their evaporation (Huff and Stout, 1964; Baechmann et al., 1996a, b; Gong et al., 2011); or an
393 increase in scavenging efficiency due to the reduction of droplet size distribution implying a larger effective
394 surface of capture (e.g., Jones et al., 2022) as well as to a local emission phenomenon (Karşı et al., 2018).

395 The high temporal resolution of the sampling, and hence, the determination of the chemical composition of the
396 dissolved and particulate phases, allows identifying more accurately the cause of these concentration increases.

397 For rainfall events R4 and R8 (Figure 4a-e), notable increases in concentration during the rain are observed for
398 both the particulate and dissolved phases. These increases appear to be associated with higher precipitation in
399 altitudes compared to the surface, as indicated by the ceilometer measurements. A plausible explanation for these
400 observations could be the partial evaporation of raindrops as they fall, leading to a reduction in their diameter and
401 a subsequent increase in mass concentration. It is assumed that only water evaporates in this process, while the
402 chemical species contained in the raindrops remain. Consequently, the initial material removed by the droplets,
403 expressed in terms of their volume, becomes greater (Baechmann et al., 1996b). On the contrary, if the evaporation
404 of the droplets is complete as they fall, this can result in the release of aerosols into the atmosphere, thereby
405 increasing atmospheric concentrations (Huff and Stout, 1964; Gong et al., 2011). This release can then affect the
406 mass concentrations of subsequent raindrops, as falling raindrops capture the released aerosols.

407 For R6, there is also an increase in mass concentrations during rainfall, but only for some species (Figure 4f-j).
408 NO_3^- and NH_4^+ concentrations increase by a factor of 4 to 5, while dissolved Zn and Cu concentrations increase
409 by a factor of 5 to 16 (included in the "others" category in Figure 2). The observed increase in NO_3^- and NH_4^+
410 mass concentrations in precipitation may be attributed to an additional input by local emissions. During this period,
411 between 7:00 and 9:00 a.m., low precipitation rates and a very low boundary layer height are observed, with the
412 cloud base height around 200 m. This specific timeframe corresponds to a period of significant road traffic, which
413 is in proximity to the monitoring site. In addition, the NO_x concentrations measured at the LISA air quality station
414 during the same time steps also display increases of more than a factor of 5. Considering that NO_x , Zn and Cu are
415 tracers of automotive activity (Thorpe and Harrison, 2008; Bukowiecki et al., 2009; Pant and Harrison, 2013), this
416 observation provides further support for the hypothesis of the influence of local emissions (in this case road traffic)
417 on the increase in mass concentrations of wet deposition throughout the event. R6 is therefore a good case study
418 to illustrate the combined influence of changing meteorological parameters and local sources on the evolution of
419 deposition concentrations during a rain event.



420

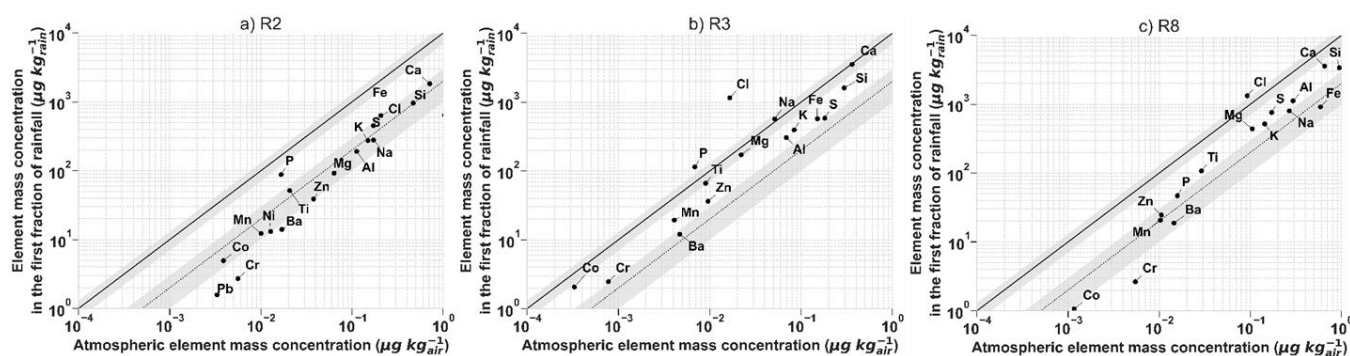
421 **Figure 4. R8 (a-e) and R6 (f-j) case studies. Evolution of PM₁₀ and PM_{2.5} concentrations (µg m⁻³; a and f) with time. The**
 422 **different sampling periods for each rain fraction are indicated by the intervals in blue (a and f). Evolution of dissolved**
 423 **mass concentration (mg L⁻¹; b and g), particulate mass concentrations (mg L⁻¹; c and h), rainfall intensity (R in mm h⁻¹;**
 424 **d and i) and droplet concentration (ND_d L⁻¹; e and j) throughout rain events.**

425 By conducting a comprehensive analysis of precipitation characteristics, atmospheric dynamics, and local
 426 influences, we aimed to shed light on the underlying mechanisms responsible for the observed punctual increases
 427 in mass concentrations during our study cases. Our results highlight the importance of the droplet size distribution,
 428 its evolution as well as the presence of local sources that evolve also during the rain event. Such investigations are
 429 essential to unravel the complexities of wet deposition dynamics and deepen our understanding of the intricate
 430 interactions between atmospheric particles and wet deposition processes.

431 **4.2. Washout ratios and scavenging coefficient**

432 The developed measurement strategy for both the chemical characterisation of aerosol and wet deposition (see
 433 section 2.3) enables to compare the concentrations in the air and in the first samples of rain, excluding the effect
 434 of dilution. Total mass concentrations estimated from chemical analysis of aerosol filters represent from 15 (R3)
 435 to 55% (R8) of the measured PM₁₀ mass concentration (Table 1), depending on the situations.

436 Total mass concentrations measured in the first fraction of rainfall events (0.06 to 0.10 mm) are higher when pre-
 437 rain PM₁₀ surface concentrations are greater (Table 1). However, for R2, R3 and R8, PM₁₀ concentrations are of
 438 the same order of magnitude (11.8 – 13 µg m⁻³) while total mass concentrations in their first fraction differ by a
 439 factor 1.8 (R2: 28.1 mg L⁻¹; R3: 49.8 mg L⁻¹; R8: 38.7 mg L⁻¹). The latter is higher when the PM_{2.5}/PM₁₀ ratio is
 440 lower (Table 1). This suggests that PM_{2.5} are scavenged less effectively than coarser particles (PM_{2.5-10}). R6 and
 441 R7 events are characterized by similar pre-rain PM₁₀ surface concentrations as well as similar PM_{2.5}/PM₁₀ ratios.
 442 However, R6 event shows total mass concentrations in the first fraction 2.4 times higher than R7 (68.3 mg L⁻¹).
 443 This can be explained by the long-range transport of mineral dust in altitude. Therefore, wet deposition fluxes at
 444 the beginning of rainfall seem to be primarily correlated to PM₁₀ surface concentrations and secondly to the coarse
 445 fraction (PM_{2.5-10} / PM₁₀). This is consistent with the aerosol size dependence of scavenging mechanisms and the
 446 minimal efficiency of the BCS mechanism between 0.2 and 2 µm (e.g., Wang et al., 2010).



448 **Figure 5. Element mass concentration in the first fraction of the rainfall ($\mu\text{g kg}_{\text{rain}}^{-1}$) as a function of the element mass**
 449 **concentration in the aerosol ($\mu\text{g kg}_{\text{air}}^{-1}$) of (a) R2, (b) R3 and (c) R8. The solid lines with envelopes correspond to washout**
 450 **ratios of the order of $10\,000 \pm 3\,000$, while the dashed lines with envelopes correspond to washout ratios of $2\,000 \pm 1\,000$.**

451 Figure 5 depicts the total concentration of elements (dissolved + particulate) in the first rain fraction ($\mu\text{g kg}_{\text{rain}}^{-1}$),
 452 plotted against the total concentration of elements measured in the aerosol ($\mu\text{g kg}_{\text{air}}^{-1}$) for R2, R3 and R8 rain events,
 453 the only rain samplings adapted for this comparison. According to the equation 2, the ratios in these two
 454 concentrations illustrated in Figure 5 correspond to the WR for analysed species (Supplement S6). It appears that
 455 the scavenging efficiency is clearly depend on the element. As an example, for similar particulate mass
 456 concentrations ($0.02 \mu\text{g kg}_{\text{air}}^{-1}$), we found higher P concentration in the first fraction of R2 ($88 \mu\text{g kg}_{\text{rain}}^{-1}$) in
 457 comparison with Ba ($14 \mu\text{g kg}_{\text{rain}}^{-1}$).

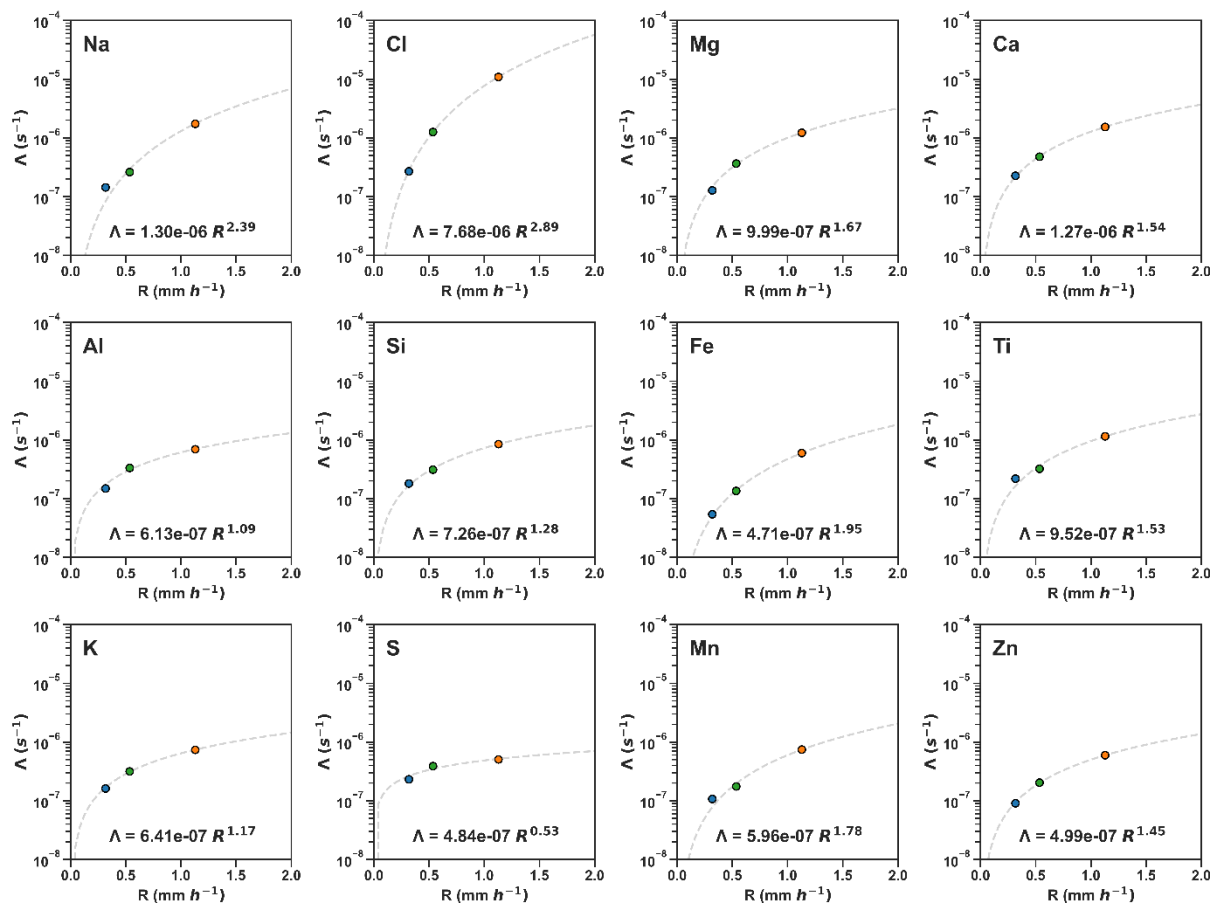
458 We found that for a given rain event, WR values can vary up to a factor of 11 to 30 from an element to another
 459 (Supplement S6). WR of elements found in R2 are primarily in the $2\,000 \pm 1\,000$ envelopes, while WR of R3 are
 460 systematically higher. Regarding R8 events, we observe an intermediate behavior in terms of WR values. In all

461 the cases, the values of WR are higher than the values previously estimated, in agreement with the dilution effect
462 on the WR available in the literature. Indeed, by taking into account the first fraction of the rainfall, the calculation
463 minimizes the influence of the ICS contribution as opposed to the WR values considering the entire event. The
464 difference of WR as a function of element could be due to either an additional source of elements in the rain (e.g.,
465 ICS or gas phase scavenging), a difference in BCS efficiency, e.g. due to different size distribution or
466 hygroscopicity of the element-bearing particles, or a contribution of PM with a diameter greater than 10 μm (e.g.,
467 Jaffrezo and Colin, 1988; Cheng et al., 2021; Kasper-Giebl et al., 1999; Cheng and Zhang, 2017). Cheng et al.
468 (2021) emphasized the predominant role of particle size distribution on the WR. Indeed, the elements associated
469 with the coarse mode ($\text{PM}_{2.5-10}$) present the largest WR, except Si and Fe, while the elements that are dominant in
470 the fine particles ($\text{PM}_{2.5}$) had lower WR. Even if we have no information on the size distribution of aerosol
471 chemical composition, the EF shows that the elements associated with coarse mode by Cheng et al. (2021) are
472 from dust origin, and those associated with fine mode (e.g., S, Zn) are of anthropogenic origin, in our samples.
473 Our results are consistent with these observations: while elements linked to coarse particles, such as calcium (WR
474 ranging between 2 500 and 9 800), exhibit higher WR values compared to those associated with fine particles,
475 such as zinc (WR ranging between 1 000 and 3 800). However, as highlighted in the review of Cheng et al. (2021),
476 some elements found primarily in the coarse mode, such as Fe (WR = 3 800), exhibit similar WR value to elements
477 associated with fine particles (e.g., Zn) as illustrated in the event R3.

478 However, our study revealed a significant variation between different events for the same chemical species.
479 Interestingly, for each element, except S, this variability consistently follows a decreasing trend in WR with
480 increasing pre-rain $\text{PM}_{2.5}/\text{PM}_{10}$ fraction (Table 1). In addition, we observed an increasing trend in WR with higher
481 rainfall rates. For instance, WR of Ca increase from 2 500 to 9 800 when rainfall rate increases from 0.5 to
482 1.2 mm h^{-1} . This shows that the particle size distribution is probably not the major factor acting on particle below-
483 cloud wet scavenging. These results are particularly noteworthy because they represent the first instance of WR
484 measurements unaffected by the dilution effect.

485 Scavenging coefficients (Λ) can be determined from the WR calculation using equation (3). These estimations are
486 the first available for major and trace metals. Figure 6 illustrates Λ of elements as a function of rainfall rate. Our
487 results show that Λ increases with rainfall rate according to a power law, as previously shown in the literature
488 (e.g., Xu et al., 2019; Wang et al., 2014). At a rainfall rate of $R = 1 \text{ mm h}^{-1}$, we obtained Λ values, between 0.5
489 and $1.3 \times 10^{-6} \text{ s}^{-1}$, with the exception of chlorine. These values fall within the range ($2.6 \times 10^{-7} - 1.7 \times 10^{-6} \text{ s}^{-1}$)
490 documented for radionuclides by Sparmacher et al. (1993) for controlled experiments with similar rainfall rate and
491 aerosol diameters (0.98 and 2.16 μm). Scavenging coefficients evolution with rainfall rate that varies from one
492 element to another, with slopes ranging from 0.5 for sulphur to 2.9 for chlorine. These differences cannot be
493 attributed solely to mass concentration, particle size, or water-soluble fraction of elements. For instance, while
494 elements associated with the same aerosol types, such as Na and Cl or Al, Ti and Si, show similar behavior with
495 rainfall rate, chlorine and sulphur exhibit contrasting trends even though they are both water soluble elements.
496 Similarly, scavenging coefficients for coarse particle (e.g., Al and Si; $1.5 - 8.5 \times 10^{-7} \text{ s}^{-1}$) are comparable to those
497 for fine particle (Zn and S; $0.9 - 6 \times 10^{-7} \text{ s}^{-1}$). Aerosol scavenging does not depend on a single parameter, but is
498 governed by the interaction of several parameters including the intrinsic properties of the aerosol (size, solubility)

499 and of the precipitation (intensity, size and number of droplets). Consequently, our results underline the critical
 500 role of rainfall rates and aerosol particle properties for the determination of both WR and Λ .



501

502 **Figure 6.** Scavenging coefficient (Λ , s^{-1}) as a function of rainfall rate (R , $mm\ h^{-1}$) for studied elements.

503 **4.3. Contribution of in-cloud and below cloud scavenging**

504 The ICS_C of chemical species analyzed in the selected rains (see 2.4) are presented in Table 3. We observe
 505 significant variations in ICS_C within individual events for different chemical species, as well as different ICS_C
 506 values of the same chemical species between different events.

507 **Table 3.** Relative ICS_C contribution (ICS_C) for R1, R2, R4 and R8 events. Bold values indicate predominance of ICS_C .

Chemical species	ICS_C (%)			
	R1	R2	R4	R8
SO_4^{2-}	62	48	23	58
NO_3^-	35	55	27	57
NH_4^+	45	40	24	65
Al	44	38	20	62
Ba	37	50	26	68
Ca	21	35	16	64

Cl	36	88	20	49
Cr	44	67	30	75
Fe	37	48	26	70
K	67	41	26	70
Mg	33	33	18	57
Mn	36	41	19	71
Na	32	85	17	53
P	24	30	17	57
Pb	82	37	18	71
Si	48	31	18	61
Sr	21	33	15	60
Ti	42	29	17	69
V	37	68	59	37
Zn	59	33	18	67
Average ± std	42 ± 15	47 ± 17	23 ± 9	62 ± 9

508 For R1, R2 and R4 anthropogenic events, the elements of crustal origin found in the coarse fraction of aerosols
509 (Al, Si, Fe, Ti, Ca, Mg, Sr) are mainly deposited via BCS mechanism. This observation is consistent with previous
510 *in situ* studies conducted in urban environments, which have reported that the BCS mechanism accounts for a
511 significant proportion (ranging from 52% to 99%) of calcium wet deposition (Ge et al., 2016; Karşı et al., 2018;
512 Ge et al., 2021a; Berberler et al., 2022). The wet deposition of Mn and NH₄⁺ is mainly attributed to the BCS
513 mechanism, accounting for 55% to 87%. This corresponds to a similar range of values reported for NH₄⁺ in other
514 urban environments in Austria (65%), Turkey (60 – 95%) and China (47 – 84%) (Xu et al., 2017; Karşı et al.,
515 2018; Berberler et al., 2022; Monteiro et al., 2021; Ge et al., 2021a). In the literature, the BCSC mechanism for
516 sulfate and nitrate in urban environments shows large variations, with reported values ranging from 50% to 98%
517 (Ge et al., 2016; Xu et al., 2017; Karşı et al., 2018; Ge et al., 2021a; Monteiro et al., 2021; Berberler et al., 2022),
518 and as low as 16% for sulfate (Aikawa et al., 2014). In our study, the BCSC of sulfate and nitrate in anthropogenic
519 events varies between 38 and 77%, depending on the events. Few chemical species show a predominance of ICS
520 mechanism in the wet deposition of anthropogenic events that could possibly be influenced by seasonal factors,
521 different local sources (such as oil and wood heating systems for SO₄²⁻, Zn), gas scavenging contributions (with
522 nitrate being mainly gaseous in summer and particulates in winter) (Audoux et al., 2023), or long distance
523 transport. For instance, seasonal factor and difference in local sources explain higher ICSC for SO₄²⁻ and Zn in R1
524 in comparison with R2 and R4. In addition, the higher ICSC obtained for Na and Cl for R2 may be linked to the
525 origin of air masses coming from the Atlantic Ocean. Overall, anthropogenic events are, on average, primarily
526 influenced by the BCS mechanism, accounting for 53% to 77% of the wet deposition of chemical species.

527 In contrast, for the mixed event R8, influenced by both local sources and long-distance transport of mineral dust,
528 the majority of chemical species, except for V (37%) and Cl (49%), are predominantly deposited through the ICS
529 mechanism, accounting for 57% to 75% of their wet deposition. While the long-distance transport of mineral dust
530 may explain the pronounced contribution of the ICS mechanism for some crustal elements, it is evident that this

531 factor alone cannot account for the prevalence of ICS for all chemical species. Certain elements observed in event
532 R8, such as NH_4^+ , are not associated with mineral dust. Since the rainfall depth is higher in this case, the higher
533 ICS contribution can be due to an effective scavenging of the air column below the cloud (Ge et al., 2021a). Indeed,
534 the wet deposition that occurs after the depletion of the atmospheric column below the cloud is primarily influenced
535 by aerosol transported and scavenged within the cloud, explaining a high contribution of ICS mechanism.

536 Several factors may contribute to these differences in the observed contribution of ICS and BCS between events.
537 One key factor is the variation in meteorological conditions, including intensity, droplet size, and cloud base
538 height, as well as PM_{10} concentrations (Table 1). Numerical studies have highlighted the importance of not only
539 cloud height but also cloud thickness in the relative contribution of BCS and ICS (Kim et al., 2021; Migliavacca
540 et al., 2010; Wiegand et al., 2011). This dependence can be explained by the fact that the higher the cloud height,
541 the greater the volume of air swept by the droplets, and therefore the greater the quantity of aerosols encountered
542 by the precipitating droplets, at equal and homogeneous concentration on the atmospheric column. For example,
543 event R1 has higher PM_{10} concentrations but 2 to 4 times lower rainfall depth compared to other anthropogenic
544 events. In addition, R4 has a higher cloud base height compared to R2, which could affect the BCS_C despite the
545 higher precipitation amount and lower PM_{10} concentration. These variations in meteorological conditions and
546 atmospheric dynamic could influence BCS efficiency as well as aerosol content to be scavenged below the cloud,
547 leading to the observed discrepancies in BCS_C and ICS_C values. Consequently, the complex interactions between
548 meteorological conditions, aerosol properties, local sources and long-range transport can result in different
549 scavenging behaviors for each event, highlighting the challenge and the need of wet deposition studies.

550 **5. Conclusion**

551 Measurement campaign has been done in the south-east of the Paris agglomeration to monitor the evolution of
552 chemical composition of wet deposition with time during rainfall events. The collected rainfall events illustrate
553 contrasting situations in terms of meteorological conditions (rainfall depth and intensity), atmospheric dynamics
554 (cloud base height between 200 and 2 500 m), as well as different atmospheric PM_{10} concentrations ranging from
555 10 to more than $60 \mu\text{g m}^{-3}$, characterized by the urban environment of the study site, but also by mineral dust
556 intrusions from the Sahara. Using additional measurements, three categories of events were identified according
557 to the origin of the aerosols found in the rain: "anthropogenic" (R1 to R4), "mineral-dust" (R5 and R6) and "mixed"
558 rainfalls (R7 and R8).

559 Our study illustrates the variability of both the mass concentrations and the chemical composition of the particulate
560 and dissolved phases. For the different rains sampled, we observe a rapid decrease in mass concentrations as the
561 rain progresses. The decrease is more pronounced for the particulate fraction (up to a factor of 50) than for the
562 dissolved fraction (up to a factor of 33), regardless of the event. However, some phases of increasing mass
563 concentrations have been identified during certain events. We have proposed several hypotheses, such as local
564 sources, evaporation of droplets and increase of scavenging efficiency, that warrant the need to thoroughly
565 document the precipitation characteristics, atmospheric dynamics, and surface PM_{10} and $\text{PM}_{2.5}$ content throughout
566 the entire rainfall event.

567 Initial chemical composition of rainfall and the chemical composition of atmospheric PM₁₀ allowed us to calculate
568 washout ratios (WR) describing the very beginning of the rainfall, before the dilution effect occurs when the
569 contribution of below cloud scavenging is greater. WR varied from below 2 000 for one event to up to 10 000 for
570 another, depending on the chemical species, and consistent with an increasing trend with increasing rainfall rate.
571 Scavenging coefficients were also determined based on the WR, rainfall intensity and cloud base height. We
572 obtained values in the range of 5.4×10^{-8} to $1.1 \times 10^{-5} \text{ s}^{-1}$ for studied elements. We found a power-lawed increase of
573 the scavenging coefficient with the rainfall rate, as previously shown in the literature, indicating a greater removal
574 of particles from the atmosphere at higher rainfall intensities. However, evolutions are not directly linked to aerosol
575 size or solubility but rather to the multiple intrinsic parameters of aerosol and precipitation. The implications of
576 these results are substantial, as they emphasize the need to consider rainfall characteristics and aerosol properties
577 for accurate estimations of the scavenging process and its impact on atmospheric deposition. Such efforts will help
578 refine and develop more reliable parameterizations that can accurately represent scavenging efficiency for a wider
579 range of environmental conditions.

580 We estimate the contributions of the in-cloud scavenging (ICS) and below cloud scavenging (BCS) mechanisms
581 for some rainfall events (R1, R2, R4 and R8). The results show a significant contribution of both mechanisms,
582 with a higher contribution of the BCS mechanism, between 53 and 77% in average, for rainfall events characterized
583 by a larger anthropogenic contribution and local sources (R1, R2 and R4). However, the contributions of
584 scavenging mechanisms are as variable from one chemical species to another as they are from one rainfall to
585 another, depending on their specific sources, atmospheric dynamic and meteorological conditions. The mixed
586 event (R8), characterized by long-distance transport of mineral dust, shows a predominant contribution of the ICS
587 mechanism, from 57 to 75% depending on the chemical species. It is difficult to determine a general trend based
588 on a limited number of events, because of the complex interactions between meteorological conditions, aerosol
589 properties, local sources and long-range transport that can result in different scavenging behaviors for each event.
590 However, our findings provide new directions for future research, particularly regarding the effect of droplet size
591 distribution and the effect of cloud base height on wet deposition dynamics.

592 To gain a comprehensive understanding of the factors influencing scavenging mechanisms, further investigation
593 is necessary, including a larger data set covering a wider range of meteorological conditions and aerosol
594 characteristics. Such a comprehensive approach will enable a more robust analysis and to confirm and/or identify
595 the dominant factors that drive scavenging during rainfall events.

596 **Acknowledgment**

597 This work is performed in the framework of the research programs DATSHA supported by the French national
598 program LEFE (Les Enveloppes Fluides et Environnement) and Foundation Air Liquide, and was also supported
599 by LISA, UPC, UPEC, UMR CNRS 7583 via its internal project call. Some of the analyses (CI, XRF) presented
600 were performed with the instruments of the PRAMMICS platform OSU-EFLUVE UMS 3563.

601 **Author contributions**

602 **TA:** Conceptualization, Formal analysis, Investigation, Writing – original draft, Writing – review & editing,
603 Visualization. **BL:** Conceptualization, Investigation, Writing – review & editing, Supervision, Funding
604 acquisition, Project administration. **KD:** Formal analysis, Investigation, Writing – review & editing. **FM:**
605 Methodology, Resources. **GN:** Formal analysis, Resources. **OL:** Formal analysis. **SC:** Conceptualization, Formal
606 analysis, Project administration.

607 **Competing interests**

608 The authors declare that they have no known competing financial interests or personal relationships that could
609 have appeared to influence the work reported in this paper.

610 **References**

- 611 Aikawa, M. and Hiraki, T.: Washout/rainout contribution in wet deposition estimated by 0.5 mm precipitation
612 sampling/analysis, *Atmospheric Environment*, 43, 4935–4939, <https://doi.org/10.1016/j.atmosenv.2009.07.057>, 2009.
- 613 Aikawa, M., Kajino, M., Hiraki, T., and Mukai, H.: The contribution of site to washout and rainout: Precipitation chemistry
614 based on sample analysis from 0.5 mm precipitation increments and numerical simulation, *Atmospheric Environment*, 95, 165–
615 174, <https://doi.org/10.1016/j.atmosenv.2014.06.015>, 2014.
- 616 Airparif: Synthèse des connaissances sur les particules en Île-de-France, 2021.
- 617 Andronache, C.: Estimates of sulfate aerosol wet scavenging coefficient for locations in the Eastern United States, *Atmospheric*
618 *Environment*, 38, 795–804, <https://doi.org/10.1016/j.atmosenv.2003.10.035>, 2004.
- 619 Anil, I., Alagha, O., and Karaca, F.: Effects of transport patterns on chemical composition of sequential rain samples: trajectory
620 clustering and principal component analysis approach, *Air Quality, Atmosphere & Health*, 10, 1193–1206,
621 <https://doi.org/10.1007/s11869-017-0504-x>, 2017.
- 622 Asman, W. A. H., Jonker, P. J., Slanina, J., and Baard, J. H.: Neutralization of Acid in Precipitation and Some Results of
623 Sequential Rain Sampling, in: *Deposition of Atmospheric Pollutants: Proceedings of a Colloquium held at Oberursel/Taunus,*
624 *West Germany, 9–11 November 1981*, edited by: Georgii, H.-W. and Pankrath, J., Springer Netherlands, Dordrecht, 115–123,
625 https://doi.org/10.1007/978-94-009-7864-5_12, 1982.
- 626 Audoux, T., Laurent, B., Chevaillier, S., Féron, A., Pangui, E., Maisonneuve, F., Desboeufs, K., Triquet, S., Noyalet, G., Lauret,
627 O., and Huet, F.: Automatic sequential rain sampling to study atmospheric particulate and dissolved wet deposition,
628 *Atmospheric Environment*, 295, 119561, <https://doi.org/10.1016/j.atmosenv.2022.119561>, 2023.
- 629 Baechmann, K., Ebert, P., Haag, I., and Prokop, T.: The chemical content of raindrops as a function of drop radius—I. Field
630 measurements at the cloud base and below the cloud, *Atmospheric Environment*, 30, 1019–1025, [https://doi.org/10.1016/1352-](https://doi.org/10.1016/1352-2310(95)00409-2)
631 [2310\(95\)00409-2](https://doi.org/10.1016/1352-2310(95)00409-2), 1996a.
- 632 Baechmann, K., Ebert, P., Haag, I., Prokop, T., and Steigerwald, K.: The chemical content of raindrops as a function of drop
633 radius—II. Field experimental study on the scavenging of marked aerosol particles by raindrops sampled as a function of drop
634 size, *Atmospheric Environment*, 30, 1027–1033, [https://doi.org/10.1016/1352-2310\(95\)00325-8](https://doi.org/10.1016/1352-2310(95)00325-8), 1996b.
- 635 Basart, S., Nickovic, S., Terradellas, E., Cuevas, E., García-Pando, C. P., García-Castrillo, G., Werner, E., and Benincasa, F.:
636 The WMO SDS-WAS Regional Center for Northern Africa, Middle East and Europe, E3S Web Conf., 99, 04008,
637 <https://doi.org/10.1051/e3sconf/20199904008>, 2019.
- 638 Berberler, E., Gemici, B. T., Uçun Özel, H., Demir, T., and Karakaş, D.: Source identification of water-insoluble single
639 particulate matters in rain sequences, *Atmospheric Pollution Research*, 13, 101499, <https://doi.org/10.1016/j.apr.2022.101499>,
640 2022.

- 641 Bertrand, G., Celle-Jeanton, H., Laj, P., Rangognio, J., and Chazot, G.: Rainfall chemistry: long range transport versus below
642 cloud scavenging. A two-year study at an inland station (Opme, France), *Journal of Atmospheric Chemistry*, 60, 253–271,
643 <https://doi.org/10.1007/s10874-009-9120-y>, 2008.
- 644 Bukowiecki, N., Lienemann, P., Hill, M., Figi, R., Richard, A., Furger, M., Rickers, K., Falkenberg, G., Zhao, Y., and Cliff, S.
645 S.: Real-world emission factors for antimony and other brake wear related trace elements: size-segregated values for light and
646 heavy duty vehicles, *Environmental Science & Technology*, 43, 8072–8078, 2009.
- 647 Calvo, A. I., Pont, V., Olmo, F. J., Castro, A., Alados-Arboledas, L., Vicente, A. M., Fernández-Raga, M., and Fraile, R.: Air
648 Masses and Weather Types: A Useful Tool for Characterizing Precipitation Chemistry and Wet Deposition, *Aerosol and Air
649 Quality Research*, 12, 856–878, <https://doi.org/10.4209/aaqr.2012.03.0068>, 2012.
- 650 Celle-Jeanton, H., Travi, Y., Loÿe-Pilot, M.-D., Huneau, F., and Bertrand, G.: Rainwater chemistry at a Mediterranean inland
651 station (Avignon, France): Local contribution versus long-range supply, *Atmospheric Research*, 91, 118–126,
652 <https://doi.org/10.1016/j.atmosres.2008.06.003>, 2009.
- 653 Cerqueira, M., Pio, C., Legrand, M., Puxbaum, H., Kasper-Giebl, A., Afonso, J., Preunkert, S., Gelencsér, A., and Fialho, P.:
654 Particulate carbon in precipitation at European background sites, *Journal of Aerosol Science*, 41, 51–61,
655 <https://doi.org/10.1016/j.jaerosci.2009.08.002>, 2010.
- 656 Chamberlain, A. C.: Aspects of the deposition of radioactive and other gases and particles, *Intern. J. Air Pollution*, Vol: 3,
657 1960.
- 658 Chatterjee, A., Jayaraman, A., Rao, T. N., and Raha, S.: In-cloud and below-cloud scavenging of aerosol ionic species over a
659 tropical rural atmosphere in India, *Journal of Atmospheric Chemistry*, 66, 27–40, <https://doi.org/10.1007/s10874-011-9190-5>,
660 2010.
- 661 Cheng, I. and Zhang, L.: Long-term air concentrations, wet deposition, and scavenging ratios of inorganic ions, HNO₃, and
662 SO₂ and assessment of aerosol and precipitation acidity at Canadian rural locations, *Atmos. Chem. Phys.*, 17, 4711–4730,
663 <https://doi.org/10.5194/acp-17-4711-2017>, 2017.
- 664 Cheng, I., Al Mamun, A., and Zhang, L.: A synthesis review on atmospheric wet deposition of particulate elements: scavenging
665 ratios, solubility, and flux measurements, *Environmental Reviews*, 29, 340–353, <https://doi.org/10.1139/er-2020-0118>, 2021.
- 666 Colette, A., Andersson, C., Manders, A., Mar, K., Mircea, M., Pay, M.-T., Raffort, V., Tsyro, S., Cuvelier, C., Adani, M.,
667 Bessagnet, B., Bergström, R., Briganti, G., Butler, T., Cappelletti, A., Couvidat, F., D’Isidoro, M., Doumbia, T., Fagerli, H.,
668 Granier, C., Heyes, C., Klimont, Z., Ojha, N., Otero, N., Schaap, M., Sindelarova, K., Stegehuis, A. I., Roustan, Y., Vautard,
669 R., van Meijgaard, E., Vivanco, M. G., and Wind, P.: EURODELTA-Trends, a multi-model experiment of air quality hindcast
670 in Europe over 1990–2010, *Geoscientific Model Development*, 10, 3255–3276, <https://doi.org/10.5194/gmd-10-3255-2017>,
671 2017.
- 672 Croft, B., Lohmann, U., Martin, R. V., Stier, P., Wurzler, S., Feichter, J., Hoose, C., Heikkilä, U., van Donkelaar, A., and
673 Ferrachat, S.: Influences of in-cloud aerosol scavenging parameterizations on aerosol concentrations and wet deposition in
674 ECHAM5-HAM, *Atmospheric Chemistry and Physics*, 10, 1511–1543, <https://doi.org/10.5194/acp-10-1511-2010>, 2010.
- 675 Dépée, A., Lemaître, P., Gelain, T., Monier, M., and Flossmann, A.: Laboratory study of the collection efficiency of submicron
676 aerosol particles by cloud droplets. Part I – Influence of relative humidity, *Atmospheric Chemistry and Physics
677 Discussions*, 1–24, <https://doi.org/10.5194/acp-2020-831>, 2020.
- 678 Desboeufs, K., Journet, E., Rajot, J.-L., Chevaillier, S., Triquet, S., Formenti, P., and Zakou, A.: Chemistry of rain events in
679 West Africa: evidence of dust and biogenic influence in convective systems, *Atmospheric Chemistry and Physics*, 10, 9283–
680 9293, <https://doi.org/10.5194/acp-10-9283-2010>, 2010.
- 681 Draxler, R. R. and Rolph, G. D.: HYSPLIT (HYbrid Single-Particle Lagrangian Integrated Trajectory) Model access via NOAA
682 ARL READY Website, <http://ready.arl.noaa.gov/HYSPLIT.php>, 2012.
- 683 Duce, R. A., Liss, P. S., Merrill, J. T., Atlas, E. L., Buat-Menard, P., Hicks, B. B., Miller, J. M., Prospero, J. M., Arimoto, R.,
684 Church, T. M., Ellis, W., Galloway, J. N., Hansen, L., Jickells, T. D., Knap, A. H., Reinhardt, K. H., Schneider, B., Soudine,
685 A., Tokos, J. J., Tsunogai, S., Wollast, R., and Zhou, M.: The atmospheric input of trace species to the world ocean, *Global
686 Biogeochemical Cycles*, 5, 193–259, <https://doi.org/10.1029/91GB01778>, 1991.
- 687 Favez, O., Weber, S., Petit, J.-E., Alleman, L. Y., Albinet, A., Riffault, V., Chazeau, B., Amodeo, T., Salameh, D., Zhang, Y.,
688 Srivastava, D., Samaké, A., Aujay-Plouzeau, R., Papin, A., Bonnaire, N., Boullanger, C., Chatain, M., Chevrier, F., Detournay,
689 A., Dominik-Sègue, M., Falhun, R., Garbin, C., Ghersi, V., Grignon, G., Levigoureux, G., Pontet, S., Rangognio, J., Zhang,

690 S., Besombes, J.-L., Conil, S., Uzu, G., Savarino, J., Marchand, N., Gros, V., Marchand, C., Jaffrezo, J.-L., and Leoz-
691 Garziandia, E.: Overview of the French Operational Network for In Situ Observation of PM Chemical Composition and Sources
692 in Urban Environments (CARA Program), *Atmosphere*, 12, 207, <https://doi.org/10.3390/atmos12020207>, 2021.

693 Ge, B., Wang, Z., Gbaguidi, A. E., and Zhang, Q.: Source Identification of Acid Rain Arising over Northeast China: Observed
694 Evidence and Model Simulation, *Aerosol and Air Quality Research*, 16, 1366–1377,
695 <https://doi.org/10.4209/aaqr.2015.05.0294>, 2016.

696 Ge, B., Xu, D., Wild, O., Yao, X., Wang, J., Chen, X., Tan, Q., Pan, X., and Wang, Z.: Inter-annual variations of wet deposition
697 in Beijing from 2014–2017: implications of below-cloud scavenging of inorganic aerosols, *Atmospheric Chemistry and
698 Physics*, 21, 9441–9454, <https://doi.org/10.5194/acp-21-9441-2021>, 2021a.

699 Ge, Y., Heal, M. R., Stevenson, D. S., Wind, P., and Vieno, M.: Evaluation of global EMEP MSC-W (rv4.34) WRF (v3.9.1.1)
700 model surface concentrations and wet deposition of reactive N and S with measurements, *Geoscientific Model Development*,
701 14, 7021–7046, <https://doi.org/10.5194/gmd-14-7021-2021>, 2021b.

702 Germer, S., Neill, C., Krusche, A. V., Neto, S. C. G., and Elsenbeer, H.: Seasonal and within-event dynamics of rainfall and
703 throughfall chemistry in an open tropical rainforest in Rondônia, Brazil, *Biogeochemistry*, 86, 155–174,
704 <https://doi.org/10.1007/s10533-007-9152-9>, 2007.

705 Gong, W., Stroud, C., and Zhang, L.: Cloud Processing of Gases and Aerosols in Air Quality Modeling, *Atmosphere*, 2, 567–
706 616, <https://doi.org/10.3390/atmos2040567>, 2011.

707 González, C. M. and Aristizábal, B. H.: Acid rain and particulate matter dynamics in a mid-sized Andean city: The effect of
708 rain intensity on ion scavenging, *Atmospheric Environment*, 60, 164–171, <https://doi.org/10.1016/j.atmosenv.2012.05.054>,
709 2012.

710 Grythe, H., Kristiansen, N. I., Zwaafink, C. D. G., Eckhardt, S., Strom, J., Tunved, P., Krejci, R., and Stohl, A.: A new aerosol
711 wet removal scheme for the Lagrangian particle model FLEXPART v10, <https://doi.org/10.5194/gmd-10-1447-2017>, 2017.

712 Haefelin, M., Barthès, L., Bock, O., Boitel, C., Bony, S., Bouniol, D., Chepfer, H., Chiriac, M., Cuesta, J., Delanoë, J.,
713 Drobinski, P., Dufresne, J.-L., Flamant, C., Grall, M., Hodzic, A., Hourdin, F., Lapouge, F., Lemaître, Y., Mathieu, A., Morille,
714 Y., Naud, C., Noël, V., O'Hirok, W., Pelon, J., Pietras, C., Protat, A., Romand, B., Scialom, G., and Vautard, R.: SIRTa, a
715 ground-based atmospheric observatory for cloud and aerosol research, *Annales Geophysicae*, 23, 253–275,
716 <https://doi.org/10.5194/angeo-23-253-2005>, 2005.

717 Huff, F. A. and Stout, G. E.: Distribution of Radioactive Rainout in Convective Rainfall, *Journal of Applied Meteorology*
718 (1962-1982), 3, 707–717, 1964.

719 Jaffrezo, J.-L. and Colin, J.-L.: Rain-aerosol coupling in urban area: Scavenging ratio measurement and identification of some
720 transfer processes, *Atmospheric Environment (1967)*, 22, 929–935, [https://doi.org/10.1016/0004-6981\(88\)90270-3](https://doi.org/10.1016/0004-6981(88)90270-3), 1988.

721 Jaffrezo, J.-L., Colin, J.-L., and Gros, J.-M.: Some physical factors influencing scavenging ratios, *Atmospheric Environment*.
722 Part A. General Topics, 24, 3073–3083, [https://doi.org/10.1016/0960-1686\(90\)90486-7](https://doi.org/10.1016/0960-1686(90)90486-7), 1990.

723 Jones, A. C., Hill, A., Hemmings, J., Lemaître, P., Quérel, A., Ryder, C. L., and Woodward, S.: Below-cloud scavenging of
724 aerosol by rain: a review of numerical modelling approaches and sensitivity simulations with mineral dust in the Met Office's
725 Unified Model, *Atmospheric Chemistry and Physics*, 22, 11381–11407, <https://doi.org/10.5194/acp-22-11381-2022>, 2022.

726 Karşı, M. B. B., Yenisoy-Karakaş, S., and Karakaş, D.: Investigation of washout and rainout processes in sequential rain
727 samples, *Atmospheric Environment*, 190, 53–64, <https://doi.org/10.1016/j.atmosenv.2018.07.018>, 2018.

728 Kasahara, M., Ogiwara, H., and Yamamoto, K.: Soluble and insoluble components of air pollutants scavenged by rain water,
729 *Nuclear Instruments and Methods in Physics Research Section B: Beam Interactions with Materials and Atoms*, 118, 400–402,
730 [https://doi.org/10.1016/0168-583X\(95\)01087-4](https://doi.org/10.1016/0168-583X(95)01087-4), 1996.

731 Kasper-Giebl, A., Kalina, M. F., and Puxbaum, H.: Scavenging ratios for sulfate, ammonium and nitrate determined at Mt.
732 Sonnblick (3106m a.s.l.), *Atmospheric Environment*, 33, 895–906, [https://doi.org/10.1016/S1352-2310\(98\)00279-9](https://doi.org/10.1016/S1352-2310(98)00279-9), 1999.

733 Kim, K. D., Lee, S., Kim, J.-J., Lee, S.-H., Lee, D., Lee, J.-B., Choi, J.-Y., and Kim, M. J.: Effect of Wet Deposition on
734 Secondary Inorganic Aerosols Using an Urban-Scale Air Quality Model, *Atmosphere*, 12, 168,
735 <https://doi.org/10.3390/atmos12020168>, 2021.

- 736 Laakso, L., Grönholm, T., Rannik, Ü., Kosmale, M., Fiedler, V., Vehkamäki, H., and Kulmala, M.: Ultrafine particle
737 scavenging coefficients calculated from 6 years field measurements, *Atmospheric Environment*, 37, 3605–3613,
738 [https://doi.org/10.1016/S1352-2310\(03\)00326-1](https://doi.org/10.1016/S1352-2310(03)00326-1), 2003.
- 739 Laquer, F. C.: Sequential precipitation samplers: A literature review, *Atmospheric Environment. Part A. General Topics*, 24,
740 2289–2297, [https://doi.org/10.1016/0960-1686\(90\)90322-E](https://doi.org/10.1016/0960-1686(90)90322-E), 1990.
- 741 LCSQA: Conformité technique des appareils de mesure, Laboratoire Central de Surveillance de la Qualité de l’Air, 2021.
- 742 Lim, B., Jickells, T. D., and Davies, T. D.: Sequential sampling of particles, major ions and total trace metals in wet deposition,
743 *Atmospheric Environment. Part A. General Topics*, 25, 745–762, [https://doi.org/10.1016/0960-1686\(91\)90073-G](https://doi.org/10.1016/0960-1686(91)90073-G), 1991.
- 744 Ma, C.-J.: Chemical composition of a yellowish rainfall by the application of PIXE and micro-PIXE technique, *Nuclear
745 Instruments and Methods in Physics Research Section B: Beam Interactions with Materials and Atoms*, 251, 501–506,
746 <https://doi.org/10.1016/j.nimb.2006.07.025>, 2006.
- 747 Mamun, A. A., Cheng, I., Zhang, L., Celso, V., Dabek-Zlotorzynska, E., and Charland, J.-P.: Estimation of Atmospheric Dry
748 and Wet Deposition of Particulate Elements at Four Monitoring Sites in the Canadian Athabasca Oil Sands Region, *Journal of
749 Geophysical Research: Atmospheres*, 127, e2021JD035787, <https://doi.org/10.1029/2021JD035787>, 2022.
- 750 Marticorena, B., Chatenet, B., Rajot, J. L., Bergametti, G., Deroubaix, A., Vincent, J., Kouoi, A., Schmechtig, C., Coulibaly,
751 M., Diallo, A., Koné, I., Maman, A., NDiaye, T., and Zakou, A.: Mineral dust over west and central Sahel: Seasonal patterns
752 of dry and wet deposition fluxes from a pluriannual sampling (2006–2012), *Journal of Geophysical Research: Atmospheres*,
753 122, 1338–1364, <https://doi.org/10.1002/2016JD025995>, 2017.
- 754 Migliavacca, D. M., Teixeira, E. C., Raya Rodriguez, M. T., Wiegand, F., and Pereira, F. N.: Analysis of the sulfate aerosol
755 scavenging processes in the metropolitan area of Porto Alegre (MAPA), RS, Brazil, *Atmospheric Pollution Research*, 1, 82–
756 93, <https://doi.org/10.5094/APR.2010.011>, 2010.
- 757 Monteiro, L. R., Terzer-Wassmuth, S., Matiatos, I., Douence, C., and Wassenaar, L. I.: Distinguishing in-cloud and below-
758 cloud short and distal N-sources from high-temporal resolution seasonal nitrate and ammonium deposition in Vienna, Austria,
759 *Atmospheric Environment*, 266, 118740, <https://doi.org/10.1016/j.atmosenv.2021.118740>, 2021.
- 760 Oduber, F., Calvo, A. I., Castro, A., Blanco-Alegre, C., Alves, C., Barata, J., Nunes, T., Lucarelli, F., Nava, S., Calzolari, G.,
761 Cerqueira, M., Martín-Villacorta, J., Esteves, V., and Fraile, R.: Chemical composition of rainwater under two events of aerosol
762 transport: A Saharan dust outbreak and wildfires, *Science of The Total Environment*, 734, 139202,
763 <https://doi.org/10.1016/j.scitotenv.2020.139202>, 2020.
- 764 Okita, T., Hara, H., and Fukuzaki, N.: Measurements of atmospheric SO₂ and SO₄²⁻, and determination of the wet scavenging
765 coefficient of sulfate aerosols for the winter monsoon season over the sea of Japan, *Atmospheric Environment*, 30, 3733–3739,
766 [https://doi.org/10.1016/1352-2310\(96\)00090-8](https://doi.org/10.1016/1352-2310(96)00090-8), 1996.
- 767 Pant, P. and Harrison, R. M.: Estimation of the contribution of road traffic emissions to particulate matter concentrations from
768 field measurements: A review, *Atmospheric Environment*, 77, 78–97, <https://doi.org/10.1016/j.atmosenv.2013.04.028>, 2013.
- 769 Ryu, Y.-H. and Min, S.-K.: Improving Wet and Dry Deposition of Aerosols in WRF-Chem: Updates to Below-Cloud
770 Scavenging and Coarse-Particle Dry Deposition, *Journal of Advances in Modeling Earth Systems*, 14, e2021MS002792,
771 <https://doi.org/10.1029/2021MS002792>, 2022.
- 772 Seinfeld, J. H. and Pandis, S. N.: *Atmospheric Chemistry and Physics: From Air Pollution to Climate Change*, John Wiley &
773 Sons, 1146 pp., 2016.
- 774 Seymour, M. D. and Stout, T.: Observations on the chemical composition of rain using short sampling times during a single
775 event, *Atmospheric Environment (1967)*, 17, 1483–1487, [https://doi.org/10.1016/0004-6981\(83\)90301-3](https://doi.org/10.1016/0004-6981(83)90301-3), 1983.
- 776 Slinn, W. G. N.: Some approximations for the wet and dry removal of particles and gases from the atmosphere, *Water, Air,
777 and Soil Pollution*, 7, <https://doi.org/10.1007/BF00285550>, 1977.
- 778 Sparmacher, H., Fülber, K., and Bonka, H.: Below-cloud scavenging of aerosol particles: Particle-bound radionuclides—
779 Experimental, *Atmospheric Environment. Part A. General Topics*, 27, 605–618, [https://doi.org/10.1016/0960-1686\(93\)90218-](https://doi.org/10.1016/0960-1686(93)90218-N)
780 N, 1993.

- 781 Tanner, P. A., Tam, C. W. F., Tanner, P. A., and Tam, C. W. F.: In-Cloud Concentrations and Below-Cloud Scavenging
782 Processes in Hong Kong, China, *Environ. Chem.*, 3, 142–148, <https://doi.org/10.1071/EN05084>, 2006.
- 783 Tapiador, F. J., Checa, R., and de Castro, M.: An experiment to measure the spatial variability of rain drop size distribution
784 using sixteen laser disdrometers, *Geophysical Research Letters*, 37, <https://doi.org/10.1029/2010GL044120>, 2010.
- 785 Taylor, S. R. and McLennan, S. M.: *The continental crust: Its composition and evolution*, 1985.
- 786 Thorpe, A. and Harrison, R. M.: Sources and properties of non-exhaust particulate matter from road traffic: A review, *Science
787 of The Total Environment*, 400, 270–282, <https://doi.org/10.1016/j.scitotenv.2008.06.007>, 2008.
- 788 Vincent, J., Laurent, B., Losno, R., Bon Nguyen, E., Rouillet, P., Sauvage, S., Chevaillier, S., Coddeville, P., Ouboulmane, N.,
789 di Sarra, A. G., Tovar-Sánchez, A., Sferlazzo, D., Massanet, A., Triquet, S., Morales Baquero, R., Fournier, M., Coursier, C.,
790 Desboeufs, K., Dulac, F., and Bergametti, G.: Variability of mineral dust deposition in the western Mediterranean basin and
791 south-east of France, *Atmospheric Chemistry and Physics*, 16, 8749–8766, <https://doi.org/10.5194/acp-16-8749-2016>, 2016.
- 792 Wang, X., Zhang, L., and Moran, M. D.: Uncertainty assessment of current size-resolved parameterizations for below-cloud
793 particle scavenging by rain, *Atmos. Chem. Phys.*, 10, 5685–5705, <https://doi.org/10.5194/acp-10-5685-2010>, 2010.
- 794 Wang, X., Zhang, L., and Moran, M. D.: On the discrepancies between theoretical and measured below-cloud particle
795 scavenging coefficients for rain – a numerical investigation using a detailed one-dimensional cloud microphysics model,
796 *Atmospheric Chemistry and Physics*, 11, 11859–11866, <https://doi.org/10.5194/acp-11-11859-2011>, 2011.
- 797 Wang, X., Zhang, L., and Moran, M. D.: Development of a new semi-empirical parameterization for below-cloud scavenging
798 of size-resolved aerosol particles by both rain and snow, *Geosci. Model Dev.*, 7, 799–819, <https://doi.org/10.5194/gmd-7-799-2014>, 2014.
- 800 Wiegand, F., Pereira, F. N., and Teixeira, E. C.: Study on wet scavenging of atmospheric pollutants in south Brazil,
801 *Atmospheric Environment*, 45, 4770–4776, <https://doi.org/10.1016/j.atmosenv.2010.02.020>, 2011.
- 802 Xu, D., Ge, B., Wang, Z., Sun, Y., Chen, Y., Ji, D., Yang, T., Ma, Z., Cheng, N., Hao, J., and Yao, X.: Below-cloud wet
803 scavenging of soluble inorganic ions by rain in Beijing during the summer of 2014, *Environmental Pollution*, 230, 963–973,
804 <https://doi.org/10.1016/j.envpol.2017.07.033>, 2017.
- 805 Xu, D., Ge, B., Chen, X., Sun, Y., Cheng, N., Li, M., Pan, X., Ma, Z., Pan, Y., and Wang, Z.: Multi-method determination of
806 the below-cloud wet scavenging coefficients of aerosols in Beijing, China, *Atmospheric Chemistry and Physics*, 19, 15569–
807 15581, <https://doi.org/10.5194/acp-19-15569-2019>, 2019.
- 808 Yamagata, S., Kobayashi, D., Ohta, S., Murao, N., Shiobara, M., Wada, M., Yabuki, M., Konishi, H., and Yamanouchi, T.:
809 Properties of aerosols and their wet deposition in the arctic spring during ASTAR2004 at Ny-Alesund, Svalbard, *Atmospheric
810 Chemistry and Physics*, 10, 2009.
- 811 Yang, Q., Easter, R. C., Campuzano-Jost, P., Jimenez, J. L., Fast, J. D., Ghan, S. J., Wang, H., Berg, L. K., Barth, M. C., Liu,
812 Y., Shrivastava, M. B., Singh, B., Morrison, H., Fan, J., Ziegler, C. L., Bela, M., Apel, E., Diskin, G. S., Mikoviny, T., and
813 Wisthaler, A.: Aerosol transport and wet scavenging in deep convective clouds: A case study and model evaluation using a
814 multiple passive tracer analysis approach, *Journal of Geophysical Research: Atmospheres*, 120, 8448–8468,
815 <https://doi.org/10.1002/2015JD023647>, 2015.
- 816 Zou, C., Yang, X., Zhang, Y., and Huang, H.: Characteristics and distribution of inorganic ions in segmented precipitation and
817 contribution of below-cloud/in-cloud scavenging in Nanchang, *Air Qual Atmos Health*, 15, 903–916,
818 <https://doi.org/10.1007/s11869-022-01166-3>, 2022.
- 819